Global Meridional Overturning Circulation Estimation in a Multiscale Ensemble Filtering CDA System with Improved Atmosphere-Ocean Exchange Fluxes

Zikuan Lin[1,2,5]†, Lv Lu[1,2]†, Shaoqing Zhang[1,2,3,5*], Yingjing Jiang[1,2], Yang Gao[3,4,5], Zhengguang Zhang[1,3,5], Xiaolin Yu[1,2,3], Mingkui Li[1,2,3], Lixin Wu[1,2,3,5], Xiaopei Lin[1,2,3,5], Haijun Yang[6] and Xue Wang[1,2]

[1]Key Laboratory of Physical Oceanography, Ministry of Education/Institute for Advanced Ocean Study/Frontiers Science Center for Deep Ocean Multispheres and Earth System (FDOMES)

[2]College of Oceanic and Atmospheric Sciences, Ocean University of China, Qingdao, China

[3]Laoshan Laboratory, Qingdao, China

[4]Key Laboratory of Marine Environment and Ecology, and Frontiers Science Center for Deep Ocean Multispheres and Earth System (FDOMES), Ministry of Education, Ocean University of China, Qingdao, China

[5]Academy of Future Ocean, Ocean University of China, Qingdao, China

[6]Department of Atmospheric and Oceanic Sciences, Fudan University, Shanghai, China

Corresponding author: Shaoqing Zhang (szhang@ouc.edu.cn)

†Co-first authors contribute equally to this work.

Key Points:

- Multiscale ensemble coupled data assimilation (CDA) is used to reconstruct atmosphere and ocean mean meridional circulation structures.
- Global meridional overturning circulation (GMOC) estimation in multiscale CDA highlights balanced and coherent state estimation.
- More coherent ocean state estimation is critical for improving GMOC estimation with more ocean observations that represent richer scales.

Abstract

Reconstruction of global meridional overturning circulation (GMOC) by combining Earth observing system with coupled climate models is crucial for climate analysis and prediction initialization. However, achieving balanced and coherent incorporation of data and model dynamics is challenging. Coupled data assimilation (CDA) addresses this by leveraging coupled model dynamics and observational information. Here with a biased twin experiment framework consisting of two coupled general circulation models (CGCMs) and a newly-developed multiscale ensemble filtering CDA algorithm, this study addresses important aspects of reconstructing GMOC. Subsequently, the CDA-reconstructed GMOC achieves error reduction over 34% (4.6 Sv out of 7.4 Sv in terms of mass transport) compared to free model simulation. The CDA data-incorporation improves atmosphere-to-ocean work and ocean-to-atmosphere heat fluxes by approximately 51% (5.7 out of 11.2 GW) and 32% (24 out of 75.6 TW) respectively, while improving 6% (3.6×10^{-7} out of 63.7×10^{-7} W/kg) of diagnosed turbulence kinetic energy dissipation. Pivotal processes in GMOC estimation are examined. The residual circulation in the Antarctic Circumpolar Circulation system is reconstructed by CDA, resulting in a 34% error reduction (.14 out of .21 m^2/s). In the North Atlantic, CDA recovers the North Atlantic Deep Water index by 50% (159 out of 316 m). Historical GMOC estimation using real observations aligns well with climatology data but requiring further deep analyses. To improve the estimation in the future, the great light shall be darted on improving ocean estimation coherence by incorporating more types of observations that represent interactions of richer scales especially in retrieving tropical multiscale processes.

Plain Language Summary

Ocean tracers such as heat, salt, and carbon are carried by the global meridional overturning circulation (GMOC), conveying between the Hemispheres. However due to sparse observations and imperfect ocean model, accurately understanding of GMOC is still challenging. Data assimilation, a method combining ocean models with real observations, could produce an accurate estimation of GMOC. Unfortunately, even in datasets produced by data assimilation procedures, the behavior of GMOC is quite different. This study introduces a new data assimilation approach that incorporates atmospheric and oceanic observations within a coupled Earth system model with the capability addressing multiscale and probabilistic nature of the data incorporation process. We demonstrate that, through a balanced and coherent data integration procedure, our new approach is able to retrieve the fundamental behavior of GMOC, which is crucial for understanding the global transport of heat, salt, carbon and nutrients.

1 Introduction

The global meridional overturning circulation (GMOC) is often defined as the result obtained by zonal integration and vertical accumulation of meridional ocean volume transport in global ocean (*Wright and Stocker*, 1991). GMOC is a complex system primarily driven by multiscale and intensive air-sea interactions (*Danabasoglu et al.*, 1994; *Macdonald and Wunsch*, 1996; *Wright et al.*, 1998). In the North Atlantic and Arctic Oceans, water masses at high latitudes are cooled and sink into the ocean abyss through deep convection (*Bjerknes*, 1964; *Shaffrey and Sutton*, 2006; *H Yang et al.*, 2013). Concurrently, the Southern Ocean experiences wind-driven upwelling (*Price et al.*, 1987), while in low-latitude regions, upwelling is usually induced by mixing processes (*Thompson*, 1978). The role of GMOC in transporting substantial heat northward in both hemispheres is important, contributing to the global redistribution of heat, freshwater, carbon, and nutrients (*H L Johnson et al.*, 2019). It has been the subject of numerous studies due to its vital role in the climate system (*G C Johnson et al.*, 2021). The importance of GMOC can extend to marine ecosystems, the carbon cycle, sea-level, and extreme weather (*Lee et al.*, 2023; *R Zhang et al.*, 2019).

Historically, hydrographic sections (observations of temperature and salinity by depth at certain transections) have been repeatedly used to estimate GMOC (*Ganachaud and Wunsch*, 2000; *Lumpkin and Speer*, 2003). However, such estimation may be subject to large spatiotemporal sampling errors inherent in the one-time synoptic hydrographic sections (*Lee et al.*, 2019). The establishment of sustained monitoring programs like RAPID-MOCHA (RAPID – Meridional Overturning Circulation and Heat flux Array) (*Cunningham et al.*, 2007) and OSNAP (Overturning in the Subpolar North Atlantic Program) (*Lozier et al.*, 2017) has facilitated the data to calculate volume transport along specific latitude transects. Utilizing data along with Argo (Array for Real-Time Geostrophic Oceanography) (*Wong et al.*, 2020) and satellite altimeter records (*T Yang and Xu*, 2015), some observation-based estimations have enabled the estimation extending back to the beginning of the altimeter record in 1993 at specific latitude (*Mercier et al.*, 2015; *Perez et al.*, 2018). However, it is still an open question whether the estimated GMOC exhibits coherent variability across latitude or not (*Bingham et al.*, 2007).

The coupled general circulation models (CGCMs) are often used to fill the gap between our physical understanding of oceanic processes and observation-based estimation (*Sugiura et al.*, 2008; *S. Zhang et al.*, 2007). However, models inevitably have shortcomings in their ability to represent the physics of nature. For example, in the coarse-resolution models (nominal 1^{o} or coarser) current, which are known that simulated jet-like currents such as Kuroshio are broad and diffuse, and much weaker than the observation, sometimes even with erroneous location and vertical structure (*Ma et al.*, 2016). For high-resolution model (nominal 0.25^{o} or finer), some important processes like mixing are still unclear (*Hirschi et al.*, 2020). Therefore, the GMOC variability in current CGCMs exhibits notable systematic biases and discrepancies (*Danabasoglu et al.*, 2014; *Danabasoglu et al.*, 2016).

Given the nature of sparse observations and inaccurate numerical models, data assimilation (DA) is a suitable tool to resolve the dilemma. DA combines prior information from imperfect models with incomplete observed data to obtain the best estimation of state evolution and its uncertainty (*Jazwinski*, 2007) of atmospheric and oceanic motions (*Carrassi et al.*, 2018) as a stochastic dynamics system (*S. Zhang et al.*, 2020). Although DA in ocean model (ODA) shows increased AMOC (Atlantic Meridional Overturning Circulation) time mean agreement in strength with the RAPID mean in multiple ODA analyses, less consistence exists in their spatial structure and temporal variability (*Karspeck et al.*, 2017). Such discrepancies imply that ocean reanalysis contains too much spurious variability in its climate (*Lu et al.*, 2020). One of the main reasons for this disparity is the widespread inhomogeneous ocean observation network. Although Expendable bathythermograph (XBT) can provide heat content data in the upper 500 m since 1970s (*Cheng et al.*, 2018), the comprehensive sampling of temperature and salinity down to 2000 m depth has only been made possible by the deployment of Argo profiling floats, which began in the mid-2000s (*Wong et al.*, 2020). Consequently, most part of the ocean is unobserved below 2000 m. In ODA, the unconstrained ocean abyss can exert significant influence on the constrained regions (*Lu et al.*, 2020). To relax this issue, *Lu et al.* (2020) implemented a climatological restoring scheme for deep ocean temperature and salinity within the ODA procedure, which is identified as a crucial strategy for reconstructing AMOC mean state and variability.

Coupled data assimilation (CDA) refers to perform DA in a coupled model framework (*Penny and Hamill*, 2017; *Sugiura et al.*, 2008; *S. Zhang et al.*, 2007; *S. Zhang et al.*, 2020). This involves the joint execution of coupled model forecasts and state estimations, enabling each component of the model receives observational information from other components. Such an integrated approach facilitates the exchange of information across different model components, producing more balanced and coherent state estimation (*S. Zhang et al.*, 2020). Specifically, as GMOC is the result of intense air-sea interaction, CDA therefore can be beneficial to the estimation of GMOC.

In this study, we first develop a new data assimilation (DA) algorithm within the coupled model framework, drawing inspiration from two key concepts: the optimal proposal density (*Evensen et al.*, 2022) and the multi-timescale filtering algorithm (*Yu et al.*, 2019) including the climatological restoring scheme. This algorithm is specifically designed to tend to improve both the accuracy of state estimation and physical balance and coherence within the coupled system. Given the challenge of distinguishing authentic changes in the climate system from spurious climate drift due to incorporation of data into a model, we first perform CDA in the twin-experiment framework. In the perspective of energy budget, we can examine the behavior of atmosphere-to-ocean work and ocean thermal responses in CDA. This examination offers an overarching perspective on the physical processes in energy cycling of CDA, as they play a key role in maintaining equilibrium of GMOC (*R X Huang et al.*, 2006). Then benefit from the interhemispheric GMOC theory, which enables a more profound depiction of dynamics of distinct regions, we can provide a deeper analysis of variability in each region. Consequently, our study provides a more comprehensive assessment of the estimated GMOC in CDA products.

This paper is organized as follows. After introduction, we describe methodology in section 2, including two CGCMs and two ensemble multiscale CDA algorithms as well as experimental design used throughout this study. Section 3 briefly validates a new multiscale ensemble filtering CDA algorithm in terms of traditional error statistics. Sections 4 and 5 examines the contributions of various atmospheric and oceanic data constraints in the coupled model framework to the exchange fluxes at the air-sea interface and kinetic energy dissipation rate as well as their impacts on GMOC estimation. Section 6 examines the estimated GMOC in a 30-year CDA reanalysis with real atmosphere and ocean observations. The conclusions and discussions are given in Section 7.

2 Methodology

2.1 Two coupled Earth system models: CESM1.3 and CM2.1

In this study, we use two CGCMs, CESM1.3 and CM2.1, to detect how CDA recover the structure and variability of ocean meridional circulation by incorporating observations into assimilation models in a balance and coherent manner. Both the CESM1.3 and CM2.1 models are fully coupled global climate models that can simulate Earth's climate system, developed by the National Center for Atmospheric Research (NCAR) and Geophysical Fluid Dynamics Laboratory of National Oceanic and Atmospheric Administration (GFDL/NOAA). As important members in phases 5 and 6 of Couple Model Inter-comparison Project (CMIP5, e.g., *Taylor et al.* (2012); CMIP6, e.g., *Eyring et al.* (2016)), the CESM1.3 and CM2.1 models are capable of providing state-of-the-art computer simulations of the past, present and future climate states of the Earth. The basic model configurations are the same as in the previous CDA studies (*Lu et al.*, 2023; *Lu et al.*, 2020; *Sun et al.*, 2022), here we only comment on some relevant aspects to this study. Both models that simultaneously simulate the atmosphere, ocean, land, and sea ice of the Earth, as well as the flux exchanges at the interfaces between the components. We configure a CESM1.3 historical simulation named BHISTC5 with the resolution ne30g16 (ne30: the atmosphere and land with roughly 1° grid-spacing in 30-element spectral-element dynamical core; g16: the ocean and ice are on nominal 1° displaced pole grid of version 6) for this study. The CESM1.3 atmosphere and ocean components include the Community Atmosphere Model version 5 (CAM5) for the atmosphere, the Community Land Model version 4.0 (CLM40) for land, and the Parallel Ocean Program version 2 (POP2) for the ocean and Community Ice Code version 4 (CICE4) for sea ice. The POP2 has 60 vertical levels, while CAM5 has 30 vertical levels. The time steps of ocean and atmosphere are 1 hour and 30 minutes respectively, with a 1-hour coupling frequency between them. We chose the component set of BHISTC5 for the experiments, in which the historical radiation conditions is used as external forcing. This historical simulation is used to produce "observations" for twin experiments that will be described in section 2.3.

We use CM2.1 as the assimilation model. The CM2.1 combines atmosphere model 2.1 and land model 2.1 (AM2.1-LM2.1) with the Modular Ocean Model version 5 (MOM5) and the Sea Ice Simulator (SIS) (*Delworth et al.*, 2006; *Gnanadesikan et al.*, 2006). The atmosphere model AM2.1 is based on a finite-volume dynamical core (*Lin*, 2004) and has a horizontal resolution of 2° latitude × 2.5° longitude (same as LM2.1) with 24 vertical levels. MOM5 is configured with 50 vertical levels (22 levels of 10 m thickness each in the top 220 m) and 1°×1° horizontal B-grid resolution telescoping to ⅓° meridional spacing near the equator. SIS in the coupled model is a dynamical ice model with three vertical layers (one for snow and two for ice) and five ice-thickness categories. The time steps of ocean and atmosphere models are 2 hours and 30 minutes respectively, with a 2-hour coupling frequency between them.

For convenience of description, hereafter we briefly name CESM1.3 and CM2.1 as CESM and CM2.

2.2 A multiscale ensemble filtering CDA algorithm

Based on previous studies (*Anderson*, 2003; *Lu et al.*, 2023; *Lu et al.*, 2020; *Yu et al.*, 2019; *S. Zhang et al.*, 2007), a new multiscale ensemble filtering CDA algorithm is designed and tested in this study. The new CDA algorithm consists of following three parts.

a) The constraint of deep ocean model bias

Due to imperfect discretization and incomplete understanding for physical processes, a coupled Earth system model is always biased with the real world (*Delworth et al.*, 2006; *S. Zhang et al.*, 2009). In data assimilation, model bias is a significant obstacle to correctly extract physical modes as observations are incorporated into the model (*Dee*, 2005; *Dee and Da Silva*, 1998), especially in ocean data assimilation (ODA) (*Balmaseda and Anderson*, 2009). Particularly, given most of the oceanic observations only available in upper 2000 m, deep ocean model bias could lead to large uncertainties in ODA (*H L Johnson et al.*, 2019; *Karspeck et al.*, 2017) since the analysis of meridional circulation requires coherent ocean stratification (*Lu et al.*, 2020). Thus, the constraint of deep ocean model bias is critically important for the ocean meridional circulation study by CDA approaches that combine a coupled Earth system model with the atmospheric and oceanic observations. Here, we use the same ocean bias constraint scheme proposed by *Lu et al.* (2020), in which the climatological temperature and salinity data (*Locarnini et al.*, 2013; *Zweng et al.*, 2013) are restored into the model space by a depth-enhanced restoring strength that is identical in all MSHea_EnOI members. In the framework of multiscale data assimilation, the restoration of climatological data is an important treatment for the mean state and fixed-period seasonal cycle with observational constraint.

b) Ensemble MSHea_EnOI

Based on the ensemble adjustment Kalman filter (EAKF) framework (*Anderson*, 2003; *S. Zhang et al.*, 2007) and CM2 model, the previous study has developed an EnOI-like Multiscale High-Efficiency Approximate filtering CDA system called MSHea-EnOI-CDA (*Lu et al.*, 2023). Due to pre-structured ensemble to represent multiscale background statistics using single model integrations, the MSHea-EnOI is a high-efficiency algorithm that is suitable for high-resolution model application in case an ensemble model integration is unaffordable. However, in weather and climate predictability studies and prediction applications, the probabilistic nature needs to be addressed (*Sévellec and Drijfhout*, 2018; *D Yang et al.*, 2023). In this study, we first use the ensemble framework of EAKF to organize multi-members of MSHea-EnOI to establish an online MSHea-EnOI ensemble system, in which each member performs MSHea-EnOI independently. The corresponding DA experiment is named by putting M_{EN} as prefix (i.e., M_{EN}-CDA etc., see **Table 1**). Here, M stands for multiscale, EN stands for ensemble. While the detailed description of MSHea-EnOI can be found in *Lu et al.* (2023), here each member of MSHea-EnOI conducts a two-step local least squares filtering adjustment as expressed in Eqs. (1) and (2) of *Lu et al.* (2023) in a relatively independent manner. Each member updates its multiscale background statistics based on its own MSHea-EnOI assimilation results.

c) MSHea_EnOI-EAKF

As discussed in *Yu et al.* (2019), while the model resolution is not too high and an affordable ensemble model integrations are available, further filtering with EAKF can improve data assimilation quality by improving statistical parameters in high-frequency filtering. In this study, when the computation of all members of ensemble MSHea_EnOI are completed, we readily conduct the EAKF filtering by collecting MSHea_EnOI ensemble results to form the ensemble analysis vector for further EAKF adjustment (*S. Zhang et al.*, 2007). We may call such a new DA algorithm that combines MSHea_EnOI (*Lu et al.*, 2023) and EAKF (*Anderson*, 2003) as MSHea_EnOI-EAKF. The corresponding DA experiment is named by putting M_{EF} as prefix (i.e., M_{EF}-CDA etc., see **Table 1**). Here, while M again stands for multiscale, EF stands for further ensemble filtering. The rationality of this approach lies in using MSHea_EnOI on each ensemble member of EAKF as a proposal density (*Evensen et al.*, 2022). Subsequently, all prior ensemble members of EAKF can be closer to the observations than pure prior samples from model integrations. Given the multi-scale characteristics of geophysical fluid, such proposed samples also maintained physical sense. We will discuss more on this point in Section 2.4.

The ensemble update equation of multiscale ensemble CDA algorithms used in this study can be divided into two steps. In the first step, we perform the M_{EN}-algorithm which establishes each dynamic ensemble (DE) member by gathering the static ensembles (SE). It can be formulized as:

$$\underbrace{\Delta x_{i,DE} = \Delta x_i^{(c)} + \sum_{\tau=1}^{\Gamma} \frac{cov\left(\Delta x_{i,SE}^{(\tau)}, \Delta y_{i,SE}^{(o,\tau)}\right)}{\left(\sigma_{i,SE}^{(\tau)}\right)^2} \times \Delta y_{i,SE}^{(o,\tau)}}_{M_{EN}\text{-algorithm}} . \quad (1)$$

Then, based on the M_{EN}-algorithm gained dynamical ensemble, we conduct EAKF filtering:

$$\underbrace{\Delta x_i = \frac{cov(\Delta x_{DE}, \Delta y_{DE}^{(o)})}{\sigma_{DE}^2} \times \Delta y_{i,DE}^{(o)}}_{M_{EF}\text{-algorithm}} . \quad (2)$$

Here, Δx and Δy represent the adjusted increment of model state variable and observational increment computed by the corresponding ensemble information (see the observational increment formulae in *Yu et al.* (2019) and *S. Zhang et al.* (2007)), respectively. The subscript i represents the ensemble member index, SE and DE stand for static ensemble pre-prepared but keeping updated with individual ensemble members and dynamical ensemble instantaneously evaluated by model integrations. The superscript (o) indicates observational information, (c) and (τ) represent the increments from climatology and a particular scale τ. Considering the fast-varying nature of atmosphere, in this study, we only apply $\Delta x^{(c)}$ to ODA.

2.3 Experimental design

a) Biased twin experiment design

1) Biases between CM2 and CESM

Usually, the influence of model bias on data assimilation is very difficult to detect due to the scattering nature of observations and uncertainties of model. The CM2 and CESM models are independently developed at different institutions along with their own biases toward the real world (*Delworth et al.*, 2006; *Meehl et al.*, 2019). We can use them to design biased twin experiments and simulate the scenario that a biased coupled Earth system model recovers the evolution of atmosphere and ocean states by assimilating the atmospheric and oceanic observations into the model (*Lu et al.*, 2023; *Lu et al.*, 2020; *S. Zhang et al.*, 2009). Therefore, having the knowledge of CM2 bias relative to CESM is important for this study.

In such biased twin experiments, the model bias can be well defined as the difference of long time mean between the two models. Although the ocean model version is slightly different, the fundamental features of the bias between CM2 and CESM are the same as *Lu et al.* (2023). Here we only comment on some aspects relevant to this study. Relative to CESM, the CM2 has large warm biases in sea surface temperature (SST) over the northeast Pacific, the subtropical north Atlantic, the east Indian Ocean and along the Antarctic continent, and cold biases over the subpolar Atlantic, the northwest Pacific, and the Southern Ocean. In sea surface salinity (SSS), large salty biases are observed over the south Tropical Pacific and Atlantic and the Indian Ocean, while fresh biases appear in the Arctic, northeast and southeast Pacific along the continent and the subpolar Atlantic. For the subsurface, above 100 m, the upper ocean shows a cold bais of roughly -0.25 ^{o}C and a warm bias of roughly 0.2 ^{o}C appears between 100–500 m, while the deep ocean below 500 m has -0.1 ^{o}C for cold bias. Above 1000 m, the salinity shows a salty bias of roughly 0.1 psu and a fresh bias of about -0.02 psu is observed below 1000 m. Relative to the CESM atmosphere, the CM2 atmosphere shows a large warm bias above 300 hPa and a small cold bias below 300 hPa. Obviously, such biases between the two coupled models are associated with their different dynamical core and physical parameterizations, etc. (*Delworth et al.*, 2006; *Meehl et al.*, 2019). Due to the nature of high-frequency variability of the atmosphere, for the issue of GMOC estimation, we pay particular attention to ocean model biases and their influences on results of various CDA schemes.

2) Biased twin experiments

To study how CDA estimates the ocean meridional circulation, we first use CM2 and CESM to design biased twin experiments. The atmosphere component of CESM model has a slightly higher resolution than CM2. Thus, we use its BHISTC5 simulation which is forced by historical greenhouse gas and natural aerosol (GHGNA) to define the “true” solution that produces synthetic “observations” based on 2007 Argo network. Please see Lu et al. 2020 for more detail. Then the CM2 free historical integration defines a biased simulation of the “truth” (TRUTH) as a control experiment (CTL).

Starting from the biased simulation of the "truth" GMOC, we conduct various CM2 M_{EN} and M_{EF} DA experiments with different schemes to assess how CDA recovers the "truth" GMOC. The synthetic "observations" of all DA experiments include "Argo" temperature and salinity profiles, gridded SSTs for ODA and surface pressure (Ps) for atmosphere data assimilation (ADA). The assimilation frequencies of ADA and ODA are 6 hours and 1 day respectively. All simulation and DA experiments are listed in **Table 1**. For example, again, the CTL and TRUTH are free model historical simulations from CM2 and CESM. While the M_{EN}-ADA (-ODA) has 12 ensemble members each of which assimilates the Ps ("Argo" profiles and SSTs) data produced by the CESM through MSHea_EnOI, the M_{EF}-ADA (-ODA) uses this 12-member ensemble to further conduct the EAKF for these atmospheric (oceanic) "observations." Correspondingly, the M_{EN}-CDA has 12 ensemble members each of which assimilates these atmospheric and oceanic "observations" through MSHea_EnOI along with its integration, and the M_{EF}-CDA uses this 12-member ensemble to further conduct the EAKF for these atmospheric and oceanic "observations." Note that in these twin experiments, the ocean data constraint includes the restoring of climatological data derived from the CESM TRUTH integration.

TABLE 1. List of experiments.

Expt	Model	Period	Ensemble size	Data constraint	Description
TRUTH	CESM1.3	1850-2000	1	Free historical run, no obs data	Prepare "true" states
CTL	CM2.1	1978-1983	1	Free historical run, no obs data	Reference for estimation
M_{EN}-ADA	CM2.1	1978-1982	12	CESM1.3-produced gridded Ps	Each member conducting MSHea_EnOI ADA
M_{EN}-ODA	CM2.1	1978-1982	12	CESM1.3-produced "Argo" T/S profiles and gridded SSTs, and ocean climatology	Each member conducting MSHea_EnOI ODA
M_{EN}-CDA	CM2.1	1978-1982	12	The data used in M_{EN}-ADA and M_{EN}-ODA	Each member conducting MSHea_EnOI ADA and ODA
M_{EF}-ADA	CM2.1	1978-1982	12	Same as in M_{EN}-ADA	12-member M_{EN}-ADA ensemble

					conducting EAKF
M_{EF}-ODA	CM2.1	1978-1982	12	Same as in M_{EN}-ODA	12-member M_{EN}-ODA ensemble conducting EAKF
M_{EF}-CDA	CM2.1	1978-1982	12	Same as in M_{EN}-CDA	12-member M_{EN}-CDA ensemble conducting EAKF
M_{EF}-CDA-Robs	CM2.1	1978-2022	12	ERA5 gridded Ps and real XBT/CTD/OSD/MRB and Argo T/S profiles as well as OISST, and WOA climatology	12-member M_{EN} ADA-Robs & ODA-Robs ensemble conducting EAKF

b) Assimilation Experiment using real observations

Finally, a CDA experiment using "real" observations called M_{EF}-CDA-Robs is conducted. For the purpose of studying reconstruction of GMOC, the M_{EF}-CDA-Robs applies the ERA5 (*Hersbach et al.*, 2020) surface pressure as "observations" of the atmosphere to ADA and all ocean real observations to ODA as shown in **Table 1**.

2.4 The assimilation quality of M_{EF}-CDA vs. M_{EN}-CDA

In the biased twin experiments, all the synthetic observations are sampled from the TRUTH based on the network of reanalysis and the modern Earth climate observing system. Atmosphere "observations" take the CESM Ps as gridded reanalysis format at model grids with a 2 hPa observational error and 6-hour time interval. Ocean "observations" are produced by sampling the CESM ocean temperature and salinity onto the 2010 Argo network repeatedly, and taking the gridded SSTs. The ocean observational error is 0.5 ℃ for temperature and 0.1 PSU for salinity at the surface and gradually decays by an e-folding depth of 2000 m. We use the 12-member ensemble mean to compute the assimilation error for estimated states and 12 individual members to evaluate the deviation of the assimilation errors. We summarize each the RMSE of ensemble mean and the RMSE's standard deviation of 12 ensemble members of each experiment, with statistics in last 3 years. Please see Table S1.

A thorough evaluation of errors statistics of atmosphere and ocean in various DA schemes can be found in Supplementary materials. Here we only comment on the basic part of the assimilation quality. Generally, both M_{EN}- and M_{EF}- have been successful in reducing RMSEs in comparison to CTL run. Regarding the atmosphere, the difference of Ps errors between M_{EN}- and M_{EF}- is small, and error reductions over lands are relatively small compared to ones over oceans. Among the seven twin-experiment conducted, the M_{EF}-CDA provides the most accurate estimation (RMSEs: 892 pascal, all others in 893-950 pascal, especially 1032 pascal in CTL) (**Figure. S1**). However, in the ocean, M_{EF}- exhibits a more significant reduction in RMSEs. Specifically, in upper ocean (above 2000m) where observations are more abundant, both M_{EF}-ODA and M_{EF}-CDA show substantial error reductions of 30% to 60% in temperature and salinity compared to M_{EN}-ODA and M_{EN}-CDA (RMSEs: 0.4 ^{o}C and 0.5 psu, **Figure. S3** and **Figure. S4 e, g**). In the abyss where the same climatology resorting scheme is employed, the temperature and salinity errors between M_{EN}- and M_{EF}- is nearly identical (**Figure. S4 f, h**). Our results indicating that the atmospheric mean meridional circulation (AMMC)-GMOC system in our experiment reach a quasi-equilibrium state by the end of 1979 (**Figure. S2**). Therefore, the analysis in this study mainly focuses on the statistics from the last three years.

3 The problem definition and CDA solution of GMOC estimation in a "twin" experiment framework of coupled Earth system models

3.1 The definition of problem

Excluding various dissipation mechanisms, the coupled atmosphere and ocean on the Earth can be viewed as a semi enclosed system (*Stommel*, 1961) in which the atmosphere "stirring" the ocean (*Munk*, 1950) while the ocean responds back to the atmosphere with new boundary conditions that have redistributed thermal properties (*Manabe*, 1969). If reducing the coupled atmosphere-ocean system to a two-dimensional vertical and meridional space, we can still view the atmosphere and ocean as a pair of zonally-averaged self-constrained counterparts as the AMMC and GMOC (*Wright and Stocker*, 1991; *Wright et al.*, 1998). In this case, due to the different dynamical-core and physical parameterizations in the CESM and CM2 models, they simulate a pair of balance and coherent AMMC and GMOC with different features in their own model spaces (**Figure. 1**). We see that, in both the Northern Hemisphere (NH) and Southern Hemisphere (SH), CM2 has stronger Hadley and Ferrel cells but weaker polar cell in NH than CESM (panels **a**, **c** & **e**). In terms of GMOC, the CM2 has a stronger Antarctic Circumpolar Current (ACC) system than the CESM (panels **b**, **d** & **f**). While the CM2's Northern sinking at 40^{o}N - 60^{o}N is much weaker than the CESM's, leading to CM2's weaker NADW (North Atlantic Deep Water). For the NADW region (40^{o}N - 60^{o}N), while the CESM shows a transport core centered at (1000 m, 45^{o}N) which is separate from the low latitude circulation cell, the CM2 only has a weak extension from the low latitude cell. In tropical oceans, the CM2's streamfunction has stronger meridional gradient at the equator area than the CESM's, thus CM2 appearing stronger vertical motion around the equator. Unlike the CESM's AABW (Antarctic Bottom Water) which extends much north beyond the equator, the CM2's anti-circulation in deep oceans is very weak in NH.

In our twin experiment framework described in Section 2.3, we can use **Figure. 1** to well define the GMOC estimation problem: Given the distinguishable differences of AMMC-GMOC structures in the two models (panels **e** & **f**), how the CM2-CDA system reconstructs the CESM-produced AMMC-GMOC (panels **a** & **b**) starting from the CM2-produced counterpart (panels **c** & **d**) by assimilating CESM-produced atmospheric and oceanic "observations" in a balance and coherent manner?

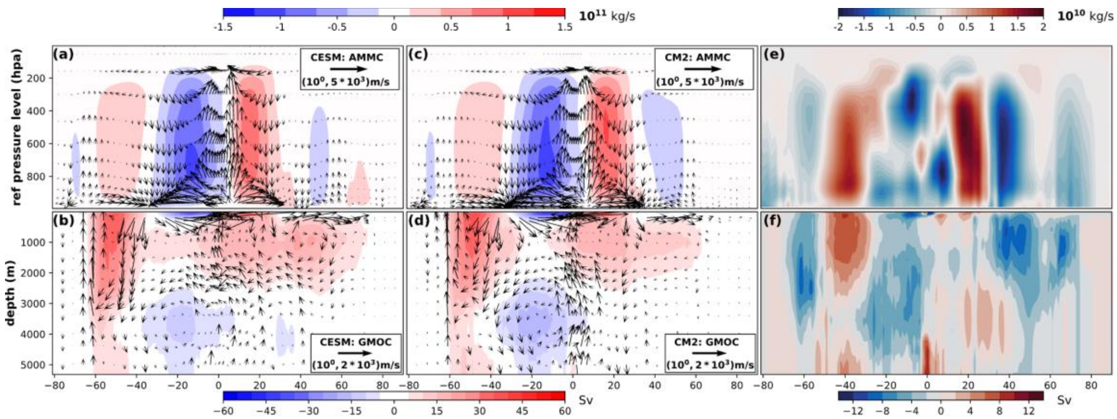

Figure. 1 AMMCs (upper) and GMOCs (lower) in the CESM and CM2 models. *a-d*) The patterns of the mean atmosphere (panels *a* & *c*) and ocean (panels *b* & *d*) meridional overturning circulation derived from zonal mean v-velocities in the y-z space as AMMCs and GMOCs, averaged over 1980-1999 in the historical simulations of CESM and CM2 starting from 1850. *e-f*) The difference between CM2 and CESM (defined as CM2 minus CESM) AMMCs (panel *e*) and GMOCs (panel *f*) shown in panels *a-d*.

3.2 The solution of CDA

The estimation of AMMC-GMOC structure by M_{EF}-CDA and the RMSE reduction rate of estimation relative to free model simulation (i.e., CTL) are shown in **Figure. 2**. We can see, through coupled atmospheric and oceanic data constraints, the stronger Hadley and Ferrel cells in CM2 has been alleviated and weaker NH polar cell has been strengthened (panels **a**). The stronger GMOC's ACC system and weaker NADW of CM2 are significantly improved (panels **b**). The error reduction rate of the AMMC is greater than 15% in most of the regions (panels **c**). A transport core in the NADW region centered at (1000 m, 45^{o}N) has been recovered, still weak though. In tropical oceans, stronger meridional gradient at the equator area has been mitigated. An anti-circulation centered at (4500 m, 40^{o}N) has been formed in deep oceans, which leads to, like the CESM, the CM2 having its AABW extended to north beyond the equator. The error reduction rate of the GMOC supports the above conclusions, surpassing 45% in ACC regions, 30% in NADW regions and 85% in AABW regions (panels **d**). However, the CDA GMOC at NH's high-latitudes and deep oceans and AMMC below 900 hPa or above 200 hPa appear error increases. Additionally. Substantial improvements are yet to be seen in addressing the strong vertical motions in tropics between 1-4 km.

While the M_{EF}-CDA offers a relatively accurate estimation of AMMC-GMOC system, it prompts new inquiries. The rationale underpinning the estimation needs to be clarified, particularly concerning the attainment of physical consistency by coupled data assimilation.

Additionally, an assessment of the uncertainties of the estimation is important. A comprehensive analysis of the estimation is therefore necessary.

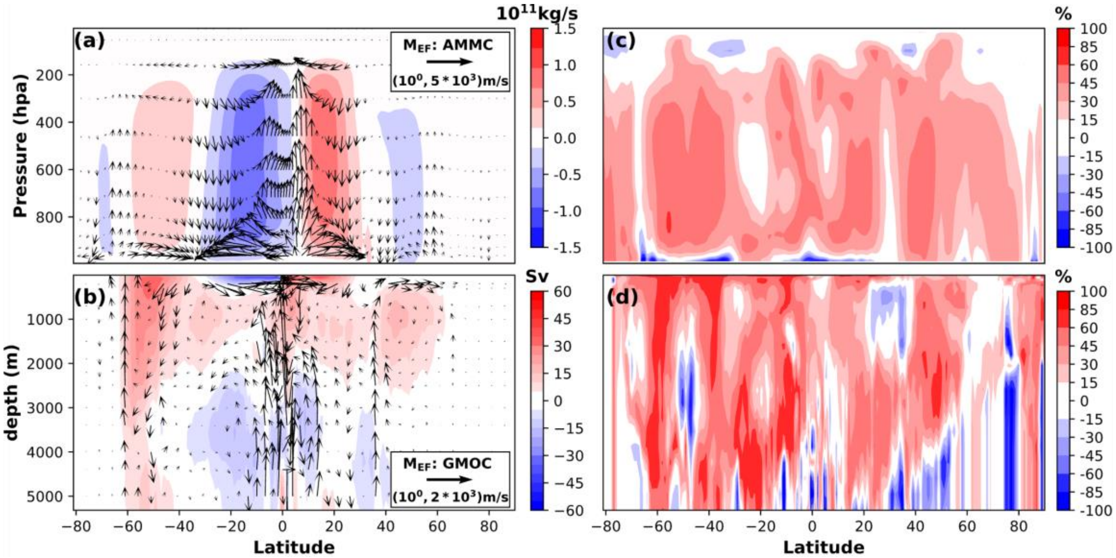

Figure. 2 The recovered AMMC and GMOC through incorporating the CESM-produced "observations" into the CM2 model by M_{EF}-CDA. a-b) Same as Figure. 1a, b but produced by M_{EF}-CDA. c-d) The reduction rate of RMSEs of AMMC (panel g) and GMOC (panel h) made by M_{EF}-CDA from the CTL ($RMSE_{CTL}$ $-RMSE_{MEF}$)/$RMSE_{CTL}$×100% (unit: %).

Next, starting to detect the roles of atmospheric and oceanic data constraints in GMOC estimation, we will try to understand the physical processes in CDA reconstruction for GMOC.

4 The detection of the roles of atmospheric and oceanic data constraints in GMOC estimation

4.1 The dynamical background of data constraints for GMOC estimation

In the regime of weak CDA, the transfer of observation information across different components primarily through fluxes. In the context of air-sea interaction, the instantaneous exchange of momentum and heat fluxes are vital to maintain global mean meridional circulation. Then given the energy, the schematic representation of the atmosphere-ocean coupling and oceanic internal responses can be depicted in **Figure. 3a**. Due to the difference of dynamical-core and physical parameterizations based their own discretization systems and physical parameterization packages, numerical models simulate a pair of balance and coherent AMMC and GMOC in their own model spaces. As atmospheric and oceanic data are incorporated into a coupled model by a CDA approach for reconstructing the AMMC-GMOC structure in the real world, the adjustment mechanism for the GMOC can be summarized and understood as the adjustment of pycnocline anomaly ($\Delta\eta$) as illustrated in **Figure. 3b**. The AMMC forces the GMOC as the consequence of the balance of three terms (*Gnanadesikan*, 1999), i.e., the difference between the Northern Hemisphere sinking and Southern Ocean upwelling is balanced by the low latitude dissipation by diffusive mixing.

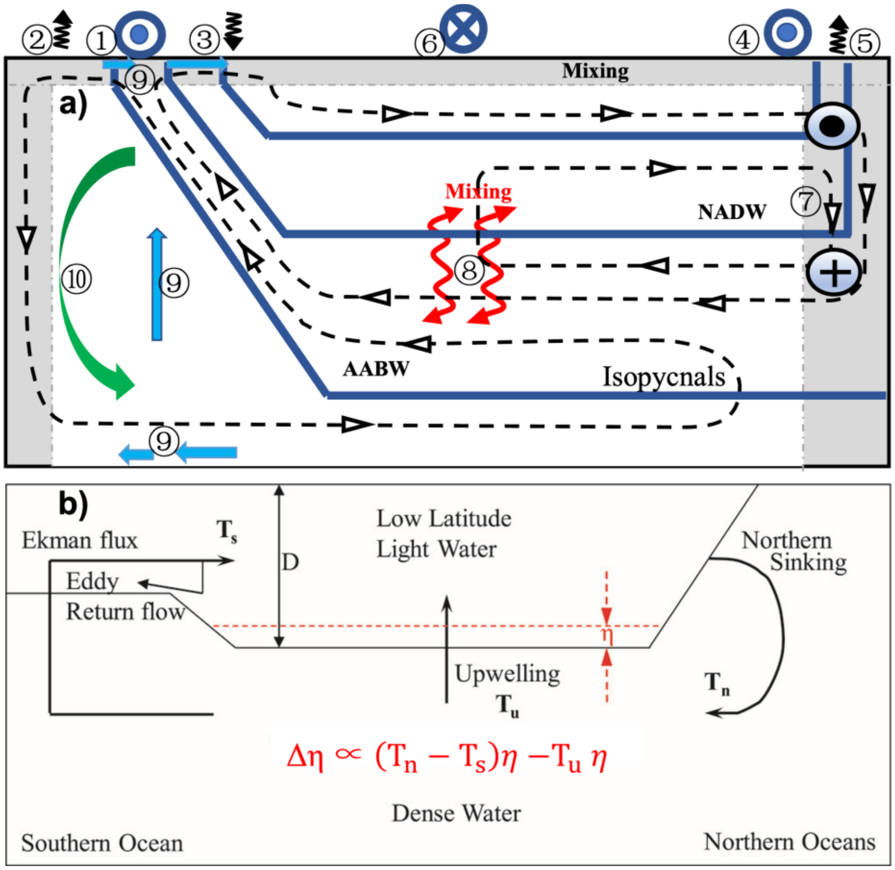

Figure. 3 The schematic illustration of processes influencing GMOC. a) Replotted from *Nikurashin and Vallis* (2012), the configuration of processes at the air-sea interface include: ① Westerly jet at the ACC region, ② Ekman effects induced buoyancy gain by ①, ③ Ekman effects induced buoyancy loss by ①, ④ Northern subpolar jet, ⑤ ④-induced buoyancy loss, ⑥ Air-sea interactions associated with Easterlies at tropics, and the configuration of ocean interior processes include: ⑦ ⑤-induced NH sinking to form North Atlantic Deep Water (NADW), ⑧ Diffusive mixing at tropical oceans, ⑨ SH wind-driven Ekman transport, ⑩ Eddy-induced circulation. ⑨ and ⑩ are important processes associated with Antarctic Bottom Water (AABW). b) Replotted from *S. Zhang* (2011), the summarized adjustment mechanism of pycnocline (Δη) from panel a as atmospheric and oceanic data are incorporated into a coupled model by a CDA approach, based on the three-term balance model of *Gnanadesikan* (1999): i.e. the residual between the difference of Northern sinking and Southern upwelling and the tropical upwelling driving the change of pycnocline depth anomaly.

The ocean primarily receives mechanical forcing from the atmosphere and reciprocally provides thermal forcing to the atmosphere, compensating for the dissipation and loss of mechanical energy caused by friction (*R X Huang et al.*, 2006). From that principle, we examine work done by atmospheric stress forces applied to the ocean (panels **a** & **d** of **Figure. 4**) and heat fluxes of ocean to the atmosphere (panels **b** & **e**) to represent the main atmosphere-ocean exchange processes (hereafter briefly referred to as W_{A2O} and HF_{O2A}).

The W_{A2O} is defined as (*R X Huang et al.*, 2006):

$$W_{A2O} = \tau_x u^o + \tau_y v^o, \#(3)$$

where τ_x (u^o) and τ_y (v^o) represent respectively the zonal and meridional components of wind stress (ocean current). The formulae to compute HF_{O2A} can be expressed as (*Cronin et al.*, 2019):

$$HF_{O2A} = Q_{sen} + Q_{lat} + Q_{lw} + Q_{sw}\ , \#(4)$$

where Q_{sen} is sensible heat flux, Q_{lat} is latent heat flux, Q_{lw} is longwave heat flux and Q_{sw} is shortwave heat flux.

Then, the AMMC-GMOC structures of CESM and CM2 models shown in **Figure. 2a-d** have their own atmosphere-ocean exchange processes at the air-sea interface. Two models share some common features in the distributions of W_{A2O} (panels **a** & **d**) and HF_{O2A} (panels **b** & **e**). On the one hand, the maximum W_{A2O} values distribute over the Southern Ocean ACC (Antarctic Circumpolar Current) belt areas and next large values mainly appear in the tropics. The former represents the major Ekman pumping effects of the atmosphere to ocean while the latter reflects the active air-sea interactions associated with warm tropical oceans. On the other hand, the maximum positive and negative values of HF_{O2A} are respectively located in tropics and high latitudes of the Northern Hemisphere, corresponding to the major heating of ocean to atmosphere at tropics (*Bernie et al.*, 2007; *Sverdrup et al.*, 1942) and cooling at jet areas of high latitudes associated with North Atlantic Oscillation (NAO) (*Delworth and Zeng*, 2016).

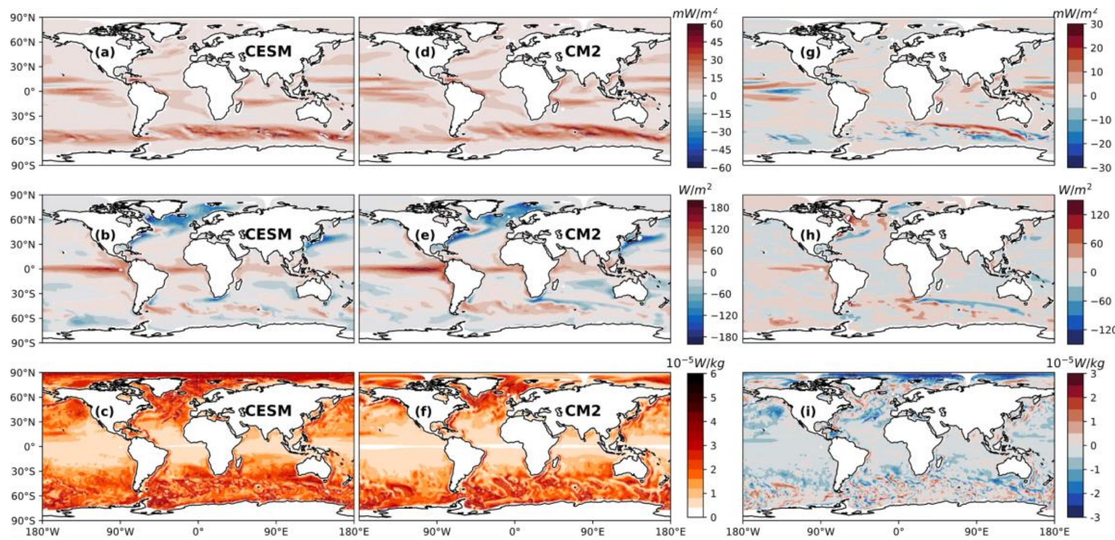

Figure. 4 Work done by atmospheric stress forces applied to the ocean (W_{A2O}) (upper), heat fluxes of ocean to the atmosphere (HF_{O2A}) (middle) and vertical mean energy dissipation rate (ε_m) (lower) in the CESM and CM models. a-f) Same as Figure. 1a-d but for the horizontal distributions of W_{A2O} (panels a & d) and HF_{O2A} (panels b & e) at the air-sea interface, as well as vertical mean energy dissipation rate (ε_m) (panels c & f). g-i) Same as Figure. 1e-f but for W_{A2O} (panel g) and HFO2A (panel h) and ε_m (panel i).

Apparently, the two models have significant differences on their W_{A2O} and HF_{O2A} distributions (panels **g** & **h**). We also see that the distributions of differences of W_{A2O} and HF_{O2A} between these two models have similar patterns with opposite sign (compare panel **g** to panel **h**), especially at high latitudes. This indicates that due to the different numerical schemes used in their atmosphere and ocean components, these two models have individually-different coupled atmosphere-ocean self-balanced regimes. In the Southern Ocean, while the CM2 has smaller atmosphere-to-ocean work than the CESM does (panel **g**), its ocean-to-atmosphere heat fluxes appear larger (panel **h**), and vice versa. The same phenomenon can be seen in the Northern Hemisphere high latitudes, particularly clear in the North Atlantic areas from the Labrador Sea to the Greenland coastal seas. In the tropics, except for the east equatorial Pacific area where CM2's smaller atmosphere-to-ocean work corresponds to larger ocean-to-atmosphere heat fluxes compared to the CESM counterparts, no clear linkage exists in the relative biases of W_{A2O} and HF_{O2A} between the two models. In the high latitudes, quasi-stationary mechanisms exist for maintenance of the Northern sinking (*Wright and Stocker*, 1991) and Southern upwelling such as wind-driven Ekman transport (*Price et al.*, 1987) at the upper oceans and eddy transports at the flanks of submarine ridges (*Macdonald and Wunsch*, 1996). To sustain the balance of three terms in GMOC (*Gnanadesikan*, 1999), each model has its own mixing processes at tropics.

Apart from flux exchanges at the air-sea interface, it's essential to check the mixing rate as they play a vital role in maintaining the global circulation (*Munk and Wunsch*, 1998). As the turbulence is not resolved in our experiment, we only compute the diagnosed turbulence kinetic energy dissipation rate. On the basis of diapycnal advection-diffusion balance:

$$\frac{D\rho}{Dt} = \frac{\partial}{\partial z}\left(\kappa_\rho \frac{\partial \rho}{\partial z}\right) = \frac{\partial}{\partial z}\left(\Gamma \varepsilon \mathrm{N}^{-2} \frac{\partial \rho}{\partial z}\right), \#(5)$$

where $N^2 = -g\rho_0^{-1}\frac{\partial \rho}{\partial z}$, w is vertical velocity, ρ is potential density, ρ_0 is the reference density, ε is diagnosed kinetic energy dissipation rate in this study. The buoyancy flux has been related to the turbulence kinetic energy dissipation rate ε through the constant efficiency factor Γ (*Osborn*, 1980). The ε on each layer therefore can be expressed as:

$$\varepsilon(z,x,y) = \int_z^0 -\frac{g}{\Gamma\rho_0}\frac{D\rho}{Dt}dz + C(x,y) \#(6)$$

In this study, we set $\Gamma = 0.2$, $\rho_0 = 1026\ kg/m^3$. The constant C is determined by letting the minimum of the integration equals to 0. The vertical mean of ε is defined as mean energy dissipation rate ε_m. ε_m in CESM and CM2 and their difference are shown in **Figure. 4c, f, i**. Although distinguishable differences exist in ε_m between CESM and CM2 (panel **i**), both models show large kinetic energy dissipation rate in the Southern Hemisphere ACC region, North Atlantic as well as Western boundary current (panels **c** & **f**). The significant dissipation in the Southern Ocean coincides with the location of maximum W_{A2O}, the substantial input of wind energy corresponding to considerable kinetic energy dissipation. The dissipation in the North Atlantic corresponds the large negative HF_{O2A} region, reflecting the cooling effect of the atmospheric jets associated with NAO, where water loses buoyancy (*Delworth and Zeng*, 2016).

Next, following the mainstream of how various DA schemes improve atmosphere-to-ocean work, ocean-to-atmosphere heat fluxes, and kinetic energy dissipation, we elaborate the contributions of ADA and ODA for recovering the target AMMC-GMOC structure to understand how a sound CDA approach reconstructs the GMOC decently.

4.2 W_{A2O} in various data constraints

We present the improvement of W_{A2O} made by M_{EF}-ADA (panel **a**) and M_{EF}-ODA (panel **b**) as well as M_{EF}-CDA (panel **c**) compared to the free model simulation of CM2 in **Figure. 5**.

Consistent with the distribution of model simulation itself, the ADA's improvement of W_{A2O} also focuses on ACC and tropical regions (panel **a**). In ODA, the improvement of W_{A2O} reflects the improvements of ocean surface current and responses of the atmosphere to improved SSTs. Such improvements depend on different geographical sensitivities to SSTs. For example, in the Southeast Atlantic, the ODA's improvement is larger than the ADA's, but in the Northwest Indian, while the ADA improves W_{A2O}, the ODA degrades it. Combining both advantages of ADA and ODA, the CDA enhances the improvement of WA2O compared to individual component DA cases (panel **c**).

We show the difference of zonal integral of W_{A2O} simulated by CESM and CM2 as well as the RMSE's reduction from the CTL made by various DA schemes in **Figure. 5d-e**. If comparing panel **e** to **d**, we see that in a zonal mean sense, the large improvement of W_{A2O} by CDA from ADA and ODA (panel e) is at the latitudes where W_{A2O} itself is large (panel d). One can see that CDA provide the most accurate estimation of W_{A2O}. In terms of the improvement from M_{EN} to M_{EF} assimilation scheme, the M_{EF} has a nearly identical behavior to the M_{EN}. (See **Figure. S5**).

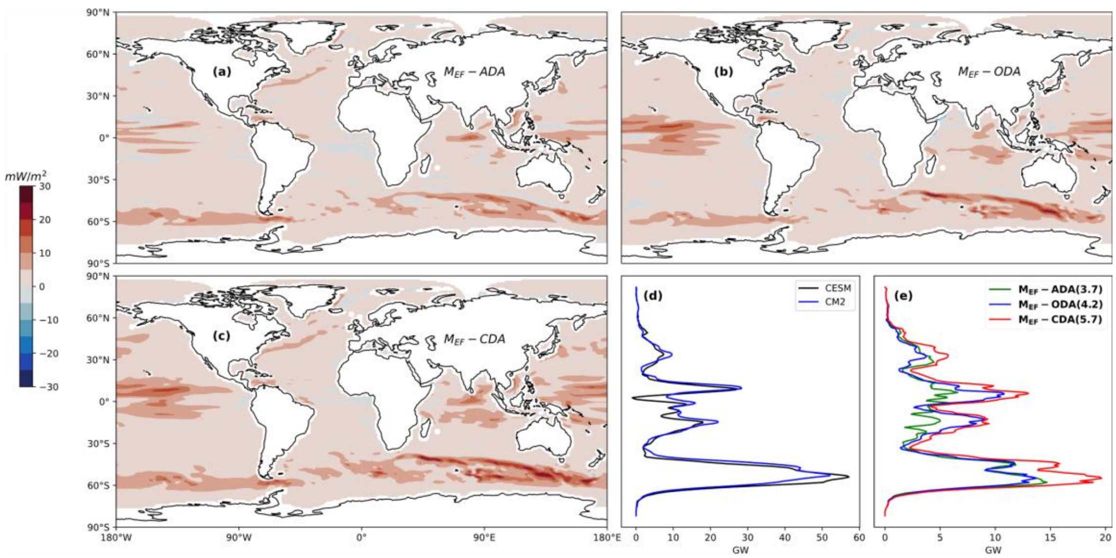

Figure. 5 The improvement of work done by atmospheric stress forces applied to the ocean made by ADA, ODA and CDA. a-c) The RMSE reduction of WA2O relative to CTL made by M_{EF}-ADA (panel a), M_{EF}-ODA (panel b) and M_{EF}-CDA (panel c) with statistics in last 3 years. d) The latitudinal variations of the zonal integral of W_{A2O} in TRUTH and CTL. e) The latitudinal variations of zonal integral of W_{A2O} error reductions from CTL (i.e., $RMSE_{CTL}$- $RMSE_{DA}$) made by M_{EF}-ADA (solid-green), M_{EF}-ODA (solid-blue) and M_{EF}-CDA (solid-red). The numbers in the parenthesis represent the latitudinal mean of error reduction of the corresponding DA experiment from the CTL (unit: GW).

4.3 HF_{O2A} in various data constraints

The story of the DA-made error reduction for HF_{O2A} (**Figure. 6**) is a little different from that for W_{A2O} shown in **Figure. 5**. As shown before, due the forcing effect of atmosphere to ocean, the distribution of error reductions of W_{A2O} in all DA schemes is overall consistent with the distribution of W_{A2O} itself, i.e., with major distributive belts over the Southern Ocean ACC and Tropical Ocean regions. The distributions of error reductions of HF_{O2A} in all DA schemes have a relatively uniform distribution in a global scope, even in the M_{EF}-ADA case (panel **a**) that represents the consequence of the response of the CM2 ocean to the ADA's constraint from CESM Ps data. Since the CM2 ocean is biased with the CESM ocean, such a response can have a global behavior. While the error reduction of HF_{O2A} made by M_{EF}-ODA (panel **b**) mainly reflects the decrease of ocean model bias shown in **Figure. 1e**, the biased nature of ocean model makes difficulties in some regions for correction with direct data constraint. Such regions include the east equatorial Pacific and Atlantic Oceans as well as the north Indian Ocean, and most of the Arctic Ocean. With the aid of ADA effects, the large errors of the east equatorial Pacific, Atlantic and north Indian Oceans appeared in ODA are greatly mitigated by CDA (panel **c**). In the tropics where the model simulated HF_{O2A} have maximum values (panel **d**), the error reductions of HF_{O2A} take the minimum values in all DA schemes. This phenomenon may be associated with the difference of two models on dealing with very active and complex air-sea interacting processes over tropical regions (*Delworth and Zeng*, 2016; *Meehl et al.*, 2019). In addition, we notice that the ODA errors in the Arctic Ocean is somewhat enlarged in CDA as the result of combining ADA and ODA together (panel **e**). This could be associated with the sea-ice behavior over the Arctic Ocean but it requires further research work to clarify.

From **Figure. 5e**, we also see that CDA produces the most accurate estimation of HF_{O2A} in ACC region and Northern Hemisphere, where the water losses buoyancy and sinks. The minimum improvement in tropics may be attributed to the strong vertical motions shown in **Figure 2**. The difference between these M_{EN} and M_{EF} algorithms is very subtle (See **Figure. S6**).

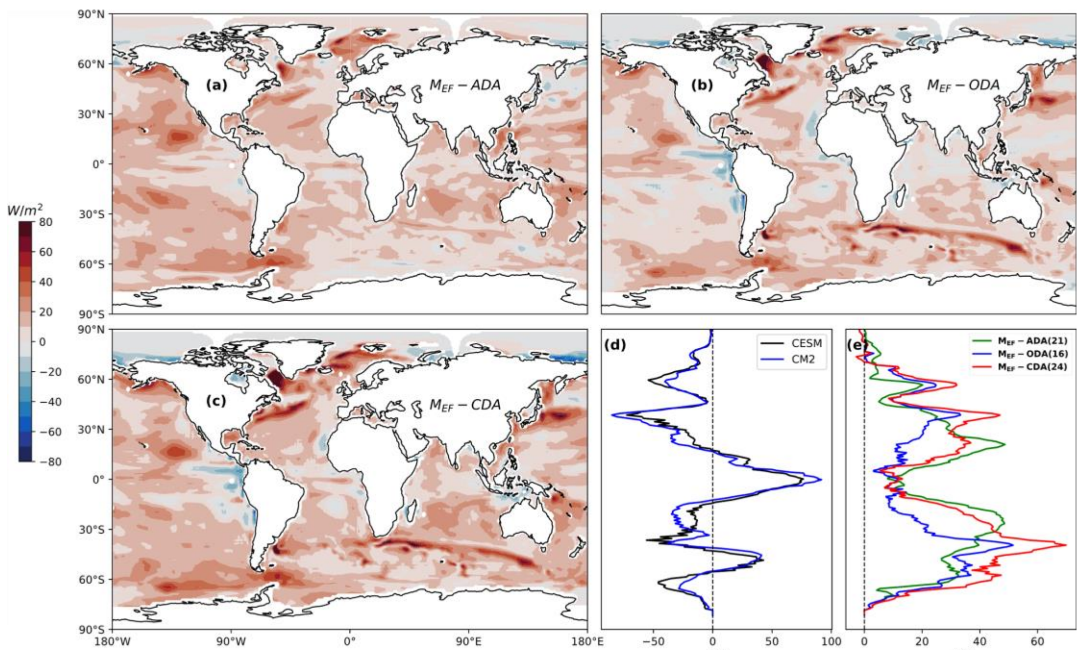

Figure. 6 The improvement of HFO2A made by ADA, ODA and CDA. a-e) Same as Figs. 5a-e but for HFO2A. The vertical dotted-black lines in panels d & e mark the zero flux (panel d) or error reduction (panel e).

4.4 ε_m in various data constraints

To understand the energy balance mechanisms of global ocean circulation (*Wunsch and Ferrari*, 2004) in CDA, we show the global distribution of the error reductions of vertical mean diagnosed turbulence kinetic energy dissipation rate (ε_m) made by various DA schemes in **Figure. 7**. As we expected, as the result of ocean free responses to atmospheric forcing, the ADA-induced ε_m appears being improved in a large scope of global domain but in a moderate magnitude without drastically-improved regions (see panel **a** and green lines in panel **e**). The direct oceanic data constraints in ODA significantly improve estimation of the ε_m over Southern Ocean where air-sea interactions are very active (panel **b**). Such improvement can be attributed to the improved estimation of stratification. However, in areas characterized by limited observation data such as the Arctic, and regions with intricate current structure like the West Boundary Currents in the West Pacific and Atlantic, ODA has difficulties to improve ε_m estimation. Combining ADA and ODA together, CDA provides a better estimation of ε_m (panel **c**). Comparing **Figure. 7 d & e** with **Figure. 6 d & e** and **Figure. 5 d & e**, we can see that in data assimilation, improving ε_m estimation is more difficult than improving W_{A2O} and HF_{O2A} since kinetic energy dissipation tightly connects with topography, convection and eddy activities etc. which easily produce modeling errors. Comparing M_{EN} to M_{EF} assimilation schemes, M_{EF}-ODA has more ε_m error reduction while M_{EF}-ADA and M_{EF}-CDA have nearly-identical behavior as the M_{EF} counterparts (See Figure. S7).

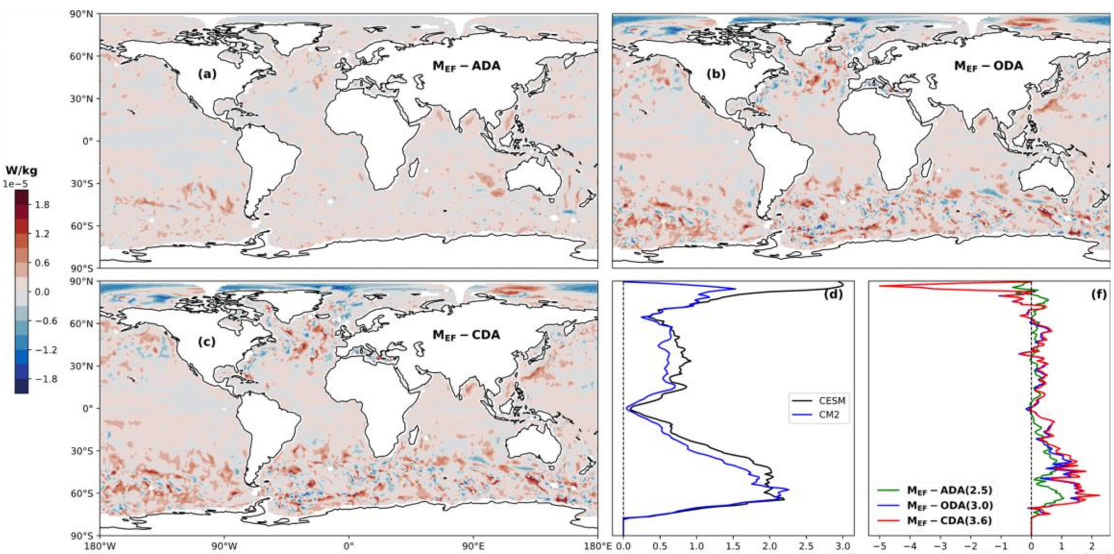

Figure. 7 The improvement of mean mixing rate (ε_m) in the global ocean made by ADA, ODA and CDA. a-e) Same as Figure. 5a-e but for ε_m described in the beginning of Section 4. The vertical dotted-black lines in panels d&e mark the zero flux (panel d) or error reduction (panel e). The numbers in the parenthesis are in unit: 10^{-7} W/kg.

5 The importance of coupled data constraints in GMOC estimation

5.1 Coupled data constraints in key processes of GMOC estimation

In this section, we focus on the results of M_{EF}-CDA to analyze the GMOC estimation. From **Figure. 3b**, we can see that the GMOC consist of three latitudinal regions: 1) high-latitudes of the Southern Hemisphere on the south of 35°S, 2) high-latitudes of the Northern Hemisphere between 40°N and 60°N, 3) tropical oceans in 20°S - 20°N. The region 1) corresponds to the ACC system linked with the processes of SH wind-driven Ekman transport and Eddy-induced circulation denoted by ⑨ and ⑩ in **Figure. 3a**, associated with AABW.

The region 2) is tightly associated with the formation mechanism of NADW linked with atmospheric jet-induced NH sinking, denoted by ⑦ in **Figure. 3a**. The region 3) corresponds to the area of diffusive mixing at tropical oceans which have active high-frequency air-sea interactions, denoted by ⑧ in **Figure. 3a**.

a) Residual circulation of ACC system

To examine the process of CDA in recovering ACC system and understand its mechanism which is important to understand CDA's GMOC (*Rintoul*, 2018), we first compute the residual circulation at high latitudes of SH. The residual circulation represents the net transport of Ekman effects but compensated by the eddy-induced circulation (*Badin and Williams*, 2010; *McIntosh and McDougall*, 1996). Following *Karsten and Marshall* (2002), the streamfunction of residual circulation (ψ^*) can be expressed as:

$$\psi^* = -\frac{\tau}{f} + K_e S, \#(7)$$

where τ and f represent wind stress and Coriolis parameter, and Ke and S are eddy diffusivity coefficient and the slope of isopycnals respectively. Then, given the zonal-mean wind stress and potential density, with $K_e = 1000\, m^2/s$ (*Visbeck et al.*, 1997), we calculate ψ^* in various DA schemes and show them in **Figure. 8**.

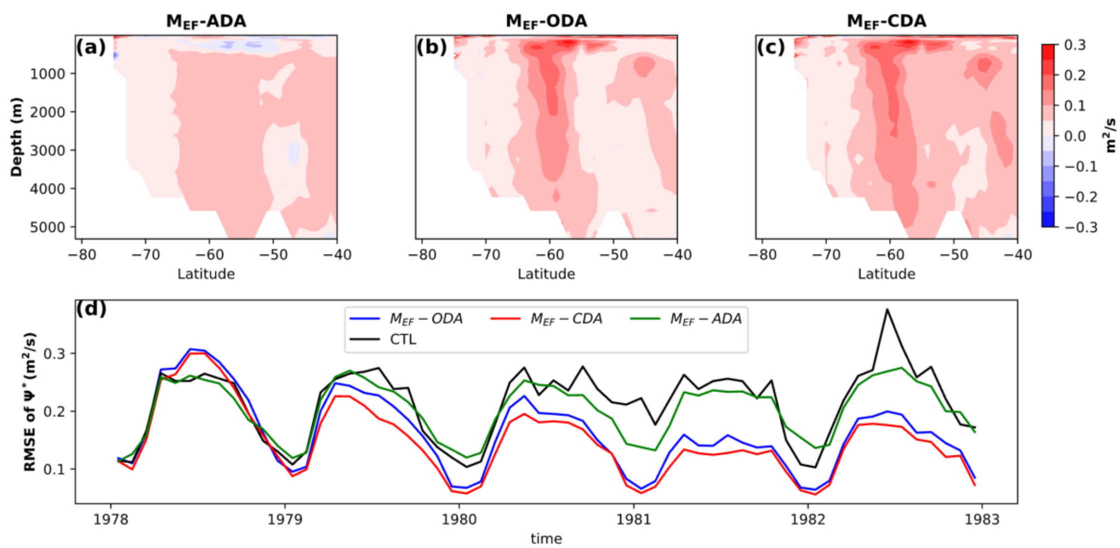

Figure. 8 The reduction of RMSEs of the residual circulation of ACC system through incorporating the CESM-produced "observations" into the CM2 model in various multiscale ensemble filtering DA approaches from the CM2 free model simulation. a-c) The RMSE reduction of ψ* made by M_{EF}-ADA (panel a), M_{EF}-ODA (panel b), M_{EF}-CDA (panel c). d) The timeseries of RMSEs of ψ* produced by M_{EF}-ADA (green), M_{EF}-ODA (blue) and M_{EF}-CDA (red). The CM2 free model control simulation (CTL) is plotted as black line as the reference.

Relying on the response of ocean to the improved $W_{A2O,}$ the ADA improves the residual circulation in a moderate magnitude (panel **a**). The slight degradation in the upper ocean above 500 m may reflects the difference of numerical schemes expressing air-sea interactions in CESM and CM2 models. The direct oceanic data constraint in ODA improves the residual circulation in much larger magnitudes than ADA with similar large-scope patterns, and particularly it corrects the upper-ocean degradation greatly (panel **b**). Taking the advantages of ODA's ability to provide a more coherent stratification and ADA's capacity to offer more accurate wind stress, the improvement of CDA for the residual circulation appears an enhanced version of the ODA (panel **c**). While exhibiting interesting spin-up features, the timeseries of RMSEs of the residual circulation in various data constraint schemes strongly support the analysis above (panel **d**). From **Figure. 8d**, we see that ODA may introduce shocks into model at the beginning period, but by the incorporation of data and model, it can quickly constrain the model state (*S. Zhang et al.*, 2009) such as the residual circulation.

b) North Atlantic Deep Water

The NADW is a good representation of low-frequency signals of North Atlantic convection (*Hopkins*, 1991; *Pickart and Spall*, 2007; *S. Zhang et al.*, 2014). Following *Pickart and Spall* (2007), we define a NADW index as the averaged thickness between two isopycnal surfaces of $\sigma_{1.5}$ over the domain of 55^{o}–35^{o}W and 45^{o}–65^{o}N where $\sigma_{1.5}$ is potential density referenced to 1500 m. In this case, we choose $\sigma_{1.5}$ = 34.52 and $\sigma_{1.5}$ = 34.62 as two isopycnal surfaces to identify North Atlantic deep mode water. We show the recovering degree of NADW by various data constraint schemes in **Figure. 9**. Unlike the role of ADA in recovering residual circulation of ACC system for which ADA greatly helps, the role of ADA in recovering NADW is very little (see panel a and green line in panel **d**), while the direct oceanic data constraint in ODA dominantly the mean state and variability of NADW (panel **b** and blue line in panel **d**). The CDA's result is nearly identical to the ODA's (panel **c** and red line in panel **d**). We may comprehend this phenomenon from two perspective. On the one hand, for slow-varying nature of NADW is primarily influenced by oceanic internal variability rather than the chaotic behavior of the atmosphere. On the other hand, this may be attributed to the large differences of two models at high-latitudes of the Northern Hemisphere in dealing with complex topography and sea-ice modeling. Therefore, it is difficult for CDA to get helps from ADA to improve the ODA's recovery in a time scale of a few years.

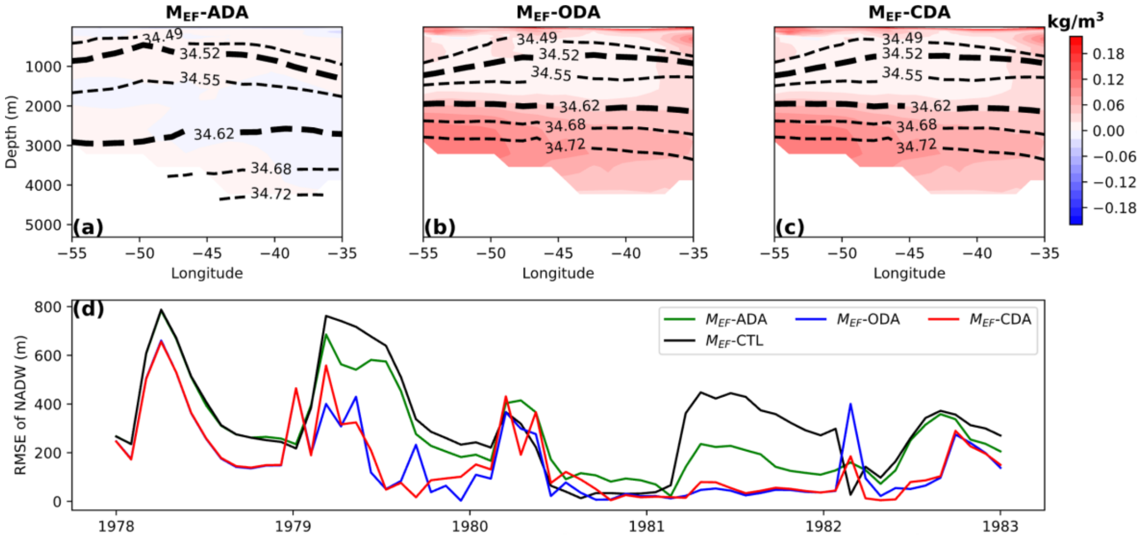

Figure. 9 The reduction of RMSEs of NADW through incorporating the CESM-produced "observations" into the CM2 model in various multiscale ensemble filtering DA approaches from the CM2 free model simulation. a-c) Same as Figure. 8 a-c but for $\sigma_{1.5}$ (potential density referenced to 1.5 km) with statistics between 45°-65°N, while the dashed lines are contours of σ1.5 averaged between 45°-65°N. defined as d) Same as Figure. 8d but for NADW [the averaged thickness between two isopycnal surfaces (34.52 and 34.62 in this case) of $\sigma_{1.5}$ over the domain of 55°–35°W and 45°–65°N].

c) Diffusive mixing at tropical oceans

The tropical oceans have very active air-sea interactions that can be in multiscale from hourly to seasonal-interannual (*Fairall et al.*, 1996; *McPhaden et al.*, 1998; *Philander*, 1990). Therefore, the tropics are an important adjuster for direct data constraints of ODA in ocean interior and they can serve as an outlet for unphysical influences of data when they are incorporated into the assimilation model as spurious signals input to the atmosphere that produces false variability. As shown in **Figure. 10**, ADA produces largest error reduction for the vertical motion of tropical oceans, and ODA is the worst, but with aids of ADA, CDA gains some mitigation from ODA. On the one hand, the free CM2 simulation has stronger vertical motions in that region (**Figure. 1d**), which suggests that CM2's dynamics favor producing strong vertical motions at tropics as the balance mechanism illustrated in **Figure. 3b**. Then, due to the great changes of NADW and ACC system in ODA's data constraints, the balance mechanism can produce such strong vertical motions in tropical 1000 – 4000 m. On the other hand, since many "malfunctions" of CM2's dynamics and physics relative to the CESM's exist, the strong vertical motion adjustment at tropical oceans could be associated with the compensation effects of such "malfunctions." For example, the sea-ice model used in CM2, SIS (sea-ice simulator) (*Winton*, 2000) is quite different from the one used in CESM, CICE5 (Community Ice Code version 5) (*Hunke et al.*, 2010). Then, the different simulations of two models at polar regions could influence on the AMMC-GMOC structure. When we incorporate the CESM-produced observations into CM2 model, such discrepancy could produce extra vertical motions at tropics as adjustment. We will discuss more on this in the Section 5.3.

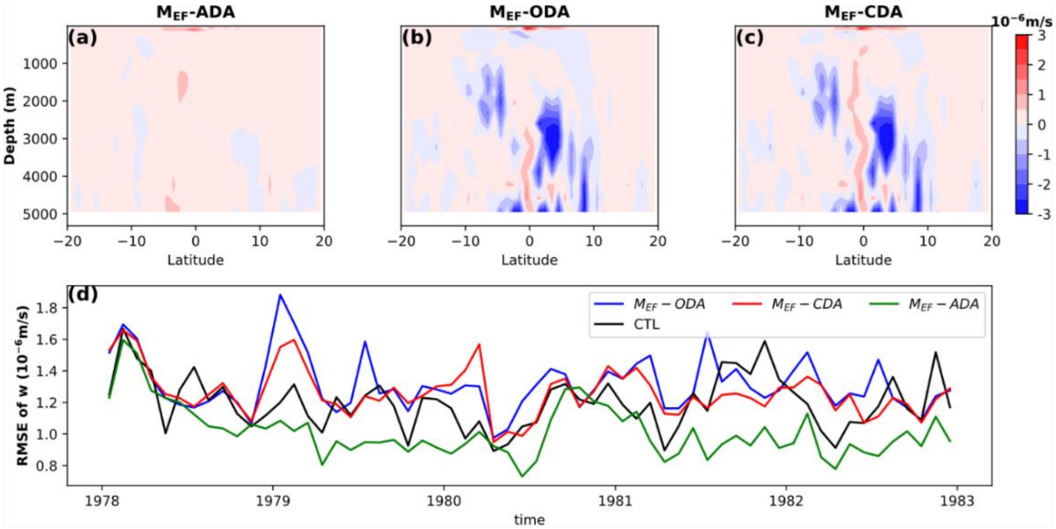

Figure. 10 The reduction of RMSEs of tropical ocean vertical motion (*w*) through incorporating the CESM-produced "observations" into the CM2 model in various multiscale ensemble filtering DA approaches from the CM2 free model simulation. *a-d* Same as Figure. 9*a-d* but for the vertical motion of tropical oceans (20^{o}S-20^{o}N).

5.2 The reconstructed AMMC-GMOC structure by coupled data constraints

In this section, we examine how the major processes described Section 5.1 reflects the efficacy of CDA in estimating the structure of AMMC-GMOC. The error reductions of AMMC-GMOC structures estimated by M_{EF}-ADA, M_{EF}-ODA and M_{EF}-CDA from the CTL are shown in **Figure. 11a-f**. Different from the model state variables such as atmosphere wind, temperature and pressure as well as ocean temperature and salinity etc. which can be directly adjusted by observational information, the AMMC and GMOC only can be derived from theses state variables. They are not only determined by the estimated values of state variables themselves, but also rely on the balanced and coherent properties among these variables (*Lu et al.*, 2020; *S. Zhang et al.*, 2014).

Generally, the incorporation of CESM-produced Ps data in M_{EN}-ADA systematically reduces the AMMC's difference between the CM2 and CESM (panel **a**). In this case, the wind in ADA is adjusted through the thermal wind geostrophic balance working on the projected vertical structure of pressure from "observational" increments of Ps data (*S. Zhang et al.*, 2014). As the consequence of CM2-ocean's responses to ADA effects through W_{A2O}, the M_{EN}-ADA estimated GMOC shows significant error reductions from the CTL in a large scope (panel **b**). But again, due to the existence of the bias of CM2-ocean vs. CESM-ocean, such responses still show light error increases in 20-40^{o}S and 1000-4000 m depths for the GMOC estimation of M_{EF}-ADA. In this case, although our deep ocean bias constraining scheme largely relaxes biases there (*Lu et al.*, 2020), the bias of CM2-ocean vs. CESM-ocean still exists. As the consequence of CM2-atmosphere responding to the ODA-improved SSTs, M_{EF}-ODA shows a globally improved AMMC (panel **c**). Nevertheless, if we compare the scope and magnitude of error reductions of AMMC and GMOC produced by M_{EF}-ADA and M_{EF}-ODA, we found that the direct data constraint in the atmosphere (ocean) makes a little smaller correction for AMMC (GMOC) than the response of atmosphere (ocean) to ODA-improved SSTs (ADA-improved sea-surface forcing). This addresses the importance of assimilating observations within the coupled model framework for estimating the AMMC-GMOC structure.

Specifically, in the ACC region (**Figure. 11**), combing M_{EF}-ADA and M_{EF}-ODA, the local maximum improvement in 60^{o}S and 40^{o}S can be attributed to the better representation of eddy-induced circulation and Ekman transport. The same degraded estimation in 50^{o}S 2– 4km can be attributed to the bias induced by climatology restoring scheme. In the north of 40^{o}N, most of the error reductions are contributed by ODA, the same as the results shown in **Figure. 9**. In tropics between 10^{o}S and 10^{o}N, although the large bias of vertical velocity at 10^{o}N still reflect on the discrepancy in GMOC, M_{EN}-ODA still produces much larger error reduction of GMOC in tropical ocean above 3.5 km. The AMMC-GMOC standard deviations, evaluating using 12 ensemble members in the M_{EF} algorithms, are presented in **Figure. 12**. These results demonstrates that the combing both atmospheric and oceanic observational data has the potential to diminish the uncertainties of data constraints. Moreover, the uncertainties of M_{EN} estimation are shown in **Figure. S8**.

To get some sense on the role of CDA in retrieving the variation of GMOC, we show the timeseries of Atlantic northward transport at 26.5^{o}N produced by various data constraints in **Figure. S9**. We see that the variation of GMOC is recovered well by CDA which coherently combines effects of atmospheric and oceanic data constraints together. Recovering variability of ocean meridional transport by CDA is critically important for both reanalysis of historical evolution of coupled Earth system and initialization of climate prediction, and thorough examination and evaluation shall be performed in the future studies.

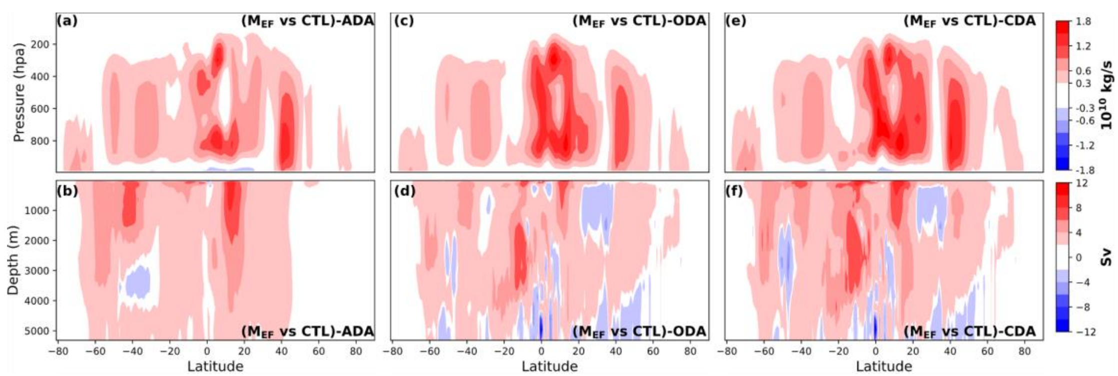

Figure. 11 The error reductions of AMMCs and GMOCs made by various ADA, ODA and CDA schemes. a-f) The RMSE reduction of AMMC (panels a, c & e) and GMOC (panels b, d & f) made by M_{EF}-ADA (panels a & b), M_{EF}-ODA (panels c & d) and M_{EF}-CDA (panels e & f) relative to the CTL's ($RMSE_{CTL}$- $RMSE_{DA}$) with statistics in last 3 years.

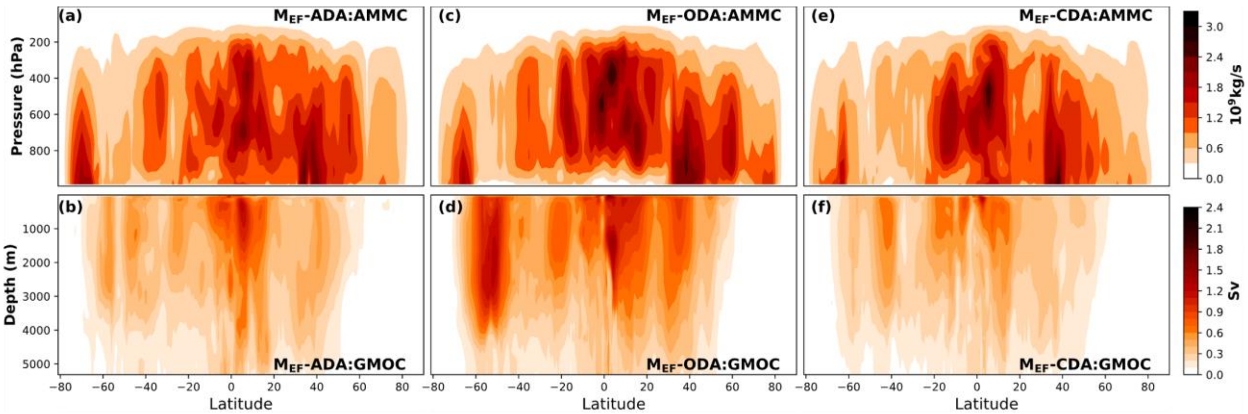

Figure. 12 The uncertainties of AMMC-GMOC estimation by various multiscale ensemble filtering DA approaches. a-f) Same as Figure. 11a-f but for ensemble standard deviation of corresponding streamfunction.

5.3 Importance of balanced and coherent coupled data constraints in GMOC estimation

The error reduction of AMMC-GMOC structures from M_{EN} to M_{EF} shows some interesting phenomenon (**Figure. 13a-f**). Generally, it is relatively easy to improve the AMMC-GMOC structure through improving atmospheric data constraint by ADA compared to improving oceanic data constraint by ODA due to less representation of ocean model and observations for complex ocean stratification. In this case, although the analyses in section 3 show the nearly-identical assimilation quality of M_{EN}-ADA and M_{EF}-ADA, the errors of both the AMMC and GMOC estimated by M_{EF}-ADA are smaller than the ones by M_{EN}-ADA, especially in tropics (panels **a** & **b**). This means that more balance and coherence exist in ADA-estimated winds and associated ocean currents. Nevertheless, while M_{EF}-ODA shows distinguishable improvement on ocean temperature and salinity relative to M_{EN}-ODA as shown in **Figure. S2**, the M_{EF}-ODA's improvement on GMOC is very limited (panel **d**). In fact, from M_{EN}-ODA to M_{EF}-ODA, the GMOC gets improved only in some tropics and middle and high latitudes of the Southern Hemisphere but degraded in almost the whole Northern Hemisphere. This suggests that improving GMOC requires more restricted spatial coherence of ocean temperature and salinity distributions. Although further ensemble filtering may extract more observational information that is mainly in the upper 2000 m, it is not necessarily true that the vertical structure of ocean is better. For AMMC, from M_{EN}-ODA to M_{EF}-ODA, the difference reflects the consequence of the atmosphere freely responding to the improved SSTs by M_{EF}-ODA, the improvement being the major message (panel **g**), particularly in the high latitudes of the Northern Hemisphere. The reconstruction of GMOC through combining observed data with a coupled model requires sufficient incorporation of atmospheric and oceanic observations into model atmospheric and oceanic states in a balanced and coherent manner.

Combining ADA and ODA, due to the addition of direct atmospheric data constraint, the ocean free responses to ADA-produced W_{A2O} significantly mitigate the degradation of M_{EF}-CDA estimated GMOC in the middle-high latitudes of the Southern Hemisphere and tropics-subtropics of the Northern Hemisphere. The maintenance of balanced physical relations between the atmosphere and ocean is very important on GMOC estimation. The atmosphere free response to ODA-produced HF_{O2A} joining with direct oceanic data constraint makes the AMMC improved in middle latitudes of the Northern Hemisphere but degraded in tropics especially low and high troposphere as well as high latitudes of the Southern Hemisphere. This phenomenon implies that the AMMC has high sensitivities to the coherent distribution of HF_{O2A}, and great light shall be darted on more coherent analysis of ocean states in the future.

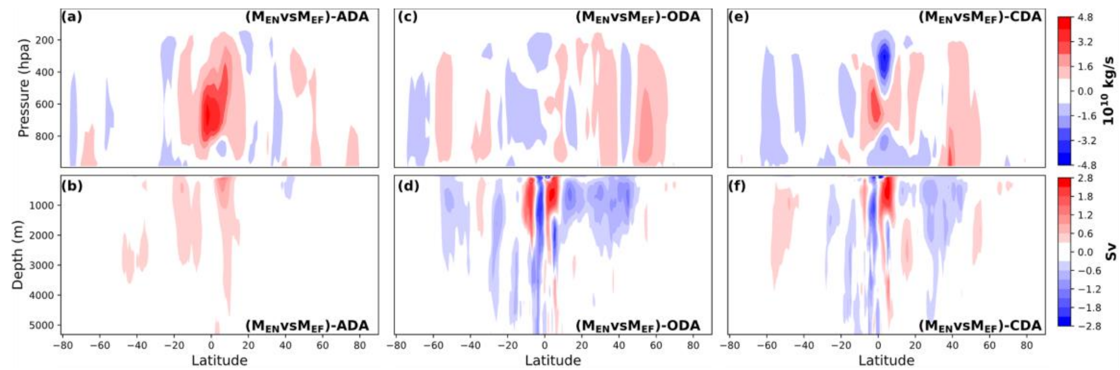

Figure. 13 The error reductions of AMMCs and GMOCs made by various ADA, ODA and CDA schemes. a-f) Same as Figure.11 a-f but made by M_{EN}-ADA (panels a & b), M_{EN}-ODA (panels c & d) and MEN-CDA (panels e & f) relative to M_{EF}-ADA, M_{EF}-ODA and M_{EF}-CDA (i.e., $RMSE_{EN}$- $RMSE_{EF}$).

We synthesize the analyses above about the roles of various data constraints in GMOC reconstruction of CDA as well as the uncertainties evaluated from the 12-member ensemble in **Figure. 14**. The improvement from southern to northern is assessed by evaluating the RMSEs improved by residual circulation in the Southern Ocean, the improved vertical velocity in tropical areas and the improvement in NADW within their geographic domains.

Within this specific “twin” experiment framework, it is shown that the CDA approach is very powerful to recover the ACC system and associated residual circulation at high latitudes of the Southern Hemisphere by incorporating the atmospheric and oceanic observations into the coupled model. In the CDA procedure, ADA (13%) helps ODA improve the recovery skill, in which while the direct oceanic data constraint in ODA recovers the residual circulation by 60%, the ADA-improved air-sea fluxes help enhance it up to 74%. The CDA skill is higher than the sum of the ADA’s and ODA’s, suggesting that positive feedback exists in the ACC system. The spread among ensemble members shows small uncertainties in the CDA procedure relative to ADA and ODA. For convection and associated NADW at high latitudes of the Northern Hemisphere, while ODA recovers 50%, ADA has a little help on them (3%) and eventually CDA recovers 52%. On the one hand, the behavior of North Atlantic convection and associated NADW has a slow-varying nature, and thus a few years of atmospheric data constraints may not be sufficient to show their effects. On the other hand, as mentioned before, large differences in topography and sea-ice modeling make difficulties for ADA to help ODA. Thus, the uncertainty of this region is larger than the Southern ACC region. Finally, CDA recovers the tropical ocean streamfunction by 2%, exhibiting a recovery capability considerably lower than ADA's (5%). However, it effectively alleviates the degradation caused by ODA (1%) in the tropical regions. The tropical diffusive mixing activities directly link with the atmosphere through frequent air-sea interactions. In the CDA framework, the residual of Southern upwelling and Northern sinking not only contains unbalanced signals of these two terms, but also includes spurious variations induced from inconsistence of data and model. The adjustment in tropical oceans can get great impacts from ADA, but as an outlet linked to the atmosphere for accumulated unbalanced information from extratropical oceans, it also contains much noises.

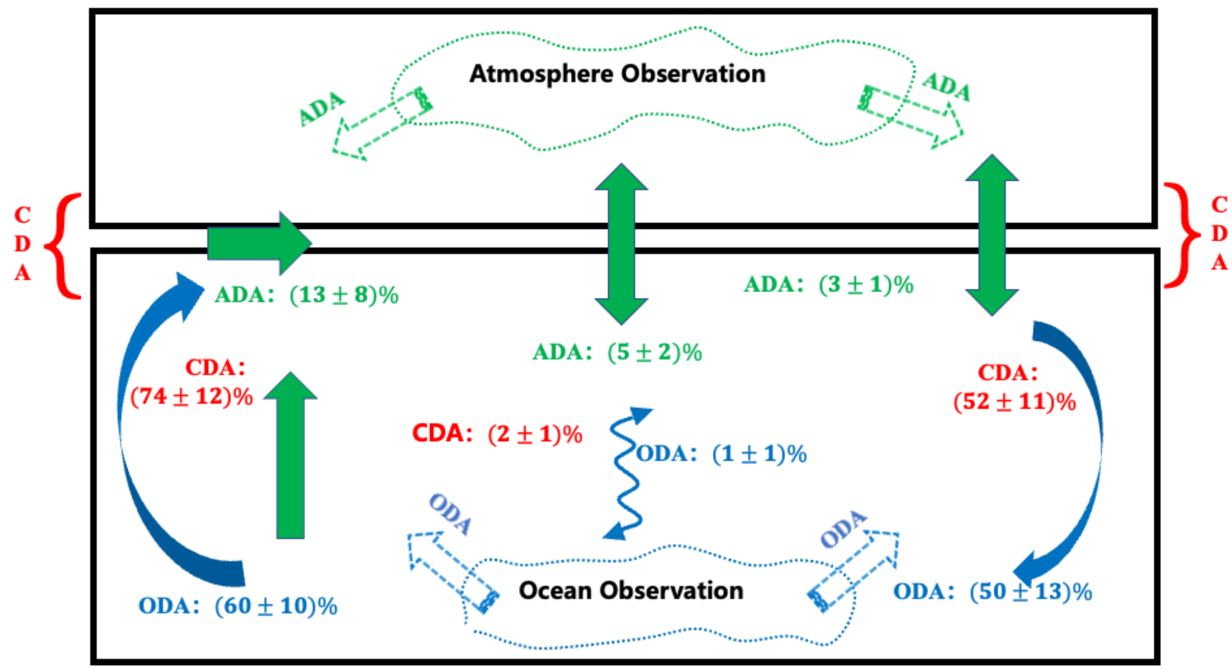

Figure. 14 The summarized illustration of relative contributions of various data constraints to GMOC estimation in CDA and their uncertainties. The illustration of oceanic (lower) [atmospheric (upper)] data constraint for the ocean (atmosphere) model by ODA and ODA's contributions (ADA and ADA's contributions) in estimation of major components of GMOC as well as their uncertainties estimated in ensemble filtering twin experiment. Curly braces indicate that a weakly-CDA approach is used in this study, which combines ADA and ODA together within the coupled model through exchanged fluxes at the air-sea interface without direct observational adjustment cross the air-sea interface.

6 The GMOC historical reanalysis by multiscale ensemble filtering CDA

To further confirm the understanding gained from the analyses of "twin" experiments on the role of multiscale ensemble filtering CDA, we conduct the "real" observation CDA experiment M_{EF}-CDA-Robs as described in Section 2.3b. The M_{EF}-CDA-Robs uses the identical ensemble initial conditions and model configuration as M_{EF}-CDA experiments in previous sections but substituting the ERA5 surface pressure (*Hersbach et al.*, 2020) and all ocean real observations described in **Table 1** as the observations of atmosphere and ocean. The results are summarized in **Figure. 15 & 16**. In general, the atmosphere and ocean state estimation converge very well (**Figure. 15a**). We notice the following phenomena. We use the HadISST product to conduct SST verification, and the RMSEs of SSTs have a little jump around 1982 because of the existence of discontinuous processing schemes in the HadISST product (*Rayner et al.*, 2003). While CDA of the M_{EF}-CDA-Robs cuts the RMSE of upper 2000 m ocean heat content by half, the timeseries show oscillations with availability of observations as well as model temporal behavior.

The M_{EF}-CDA-Robs estimated GMOC (**Figure. 15b**) appears having a large adjustment from the model control as shown in **Figure. 1d**. Usually, the GMOC in free model simulations exhibits a continuous single circulation cell above 2500 m and a weak anti-circulation cell at tropical deep ocean. Compared to the CM2 free model control simulation, the GMOC estimated by M_{EF}-CDA-Robs appears having much strengthened Northern NADW. A core of NADW is established and the weak anti-circulation at tropical deep ocean in free model simulation becomes much strong and extends to the upper ocean so that the continuous single circulation cell of GMOC becomes a double-core structure (**Figure. 15b**). The Southern ACC system also encounters some adjustment in which the Ekman transport centered at 50°S becomes weaker and anti-circulation branch in the residual circulation apparently becomes stronger. The northward transport in the Southern middle latitudes becomes stronger and a core centered at 35°S and 1000 m is formed. We may comprehend the changes of ACC system and NADW as consistent data constrained signals.

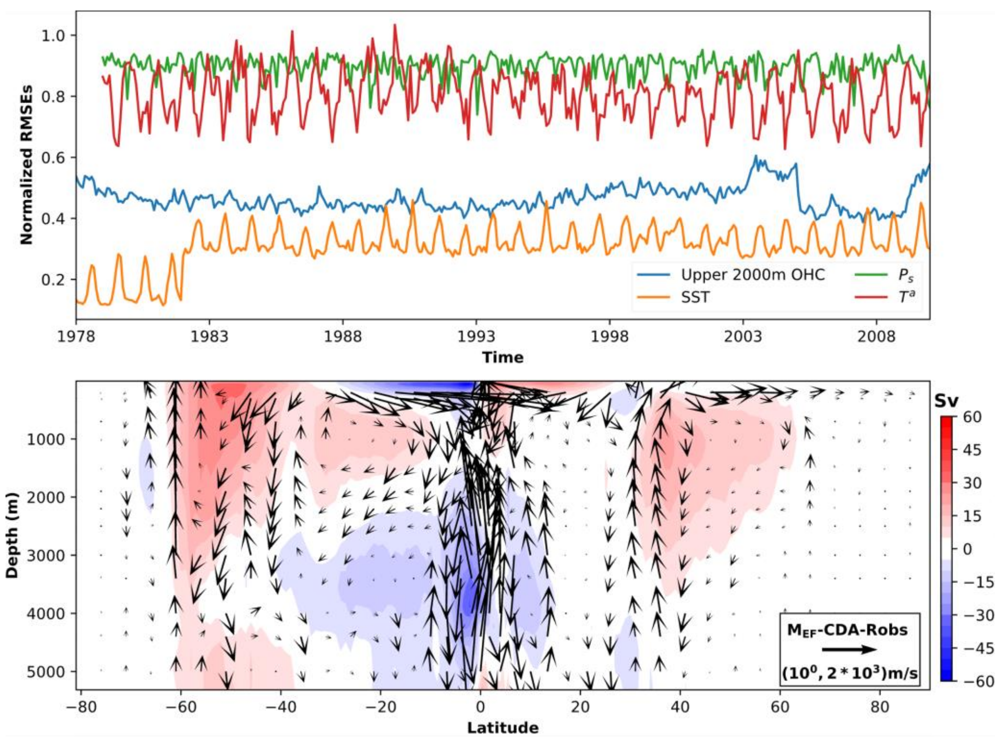

Figure. 15 The convergent atmospheric and oceanic state estimation (upper) and estimated 30-year time mean GMOC (lower) by multiscale ensemble filtering CDA approach through incorporating atmospheric and oceanic observations into CM2. a) The timeseries of normalized global RMSEs of surface pressure (Ps) (solid-green), atmosphere temperature (Ta) (solid-red), sea surface temperature (SST) (solid-yellow) and upper 2000 m ocean heat content (solid-blue) produced by M_{EF}-CDA-Robs (see Table 1), by corresponding RMSE values at the initial state. We use the HadISST and EN4 products as verification target for SST and ocean heat content. Note that to sustain ensemble filtering ODA, we activiate ADA after 1-year of ODA, and due to the existence of discontinuous processing schemes in the HadISST product, there is a little jump around 1982. b) The distribution of 1981-2010 time mean meridional streamfunctions produced by M_{EF}-CDA-Robs, configured with corresponding [v,w] vectors.

To get some insights on the signal-to-noise ratio of estimation analyses above, especially for the large tropical adjustments, we compute the time mean geostrophic GMOCs using ocean temperature and salinity profiles (*Chu*, 2000; *Chu and Fan*, 2015) produced by the CM2 free model simulation and M_{EF}-CDA-Robs and compared to the WOA13 climatological data (*Zweng et al.*, 2013; *Locarnini et al.*, 2013) (**Figure. 16**). The geostrophic flow between 7° S-7° N is done by using the following equations:

$$v = v * \left(|lat| \times \frac{|lat| - 14}{49}\right)^2, \# (8)$$

where lat is the latitude of the meridional velocity v. From **Figure. 16**, we do see the large scope improvement of geostrophic GMOC by M_{EF}-CDA-Robs indeed from the model control, except for slightly worse in small regions at 35°S and above 1000 m as well as at 15°N between 1000-4000 m. The largest improvements are found in the Southern ACC system and Northern NADW regions, which strongly support our comprehension in the analysis for the appearance of total streamfunction. Even for the tropics, the CDA procedure reduces the errors of geostrophic GMOC by a distinguishable degree (compare panel **e** to panel **d**).

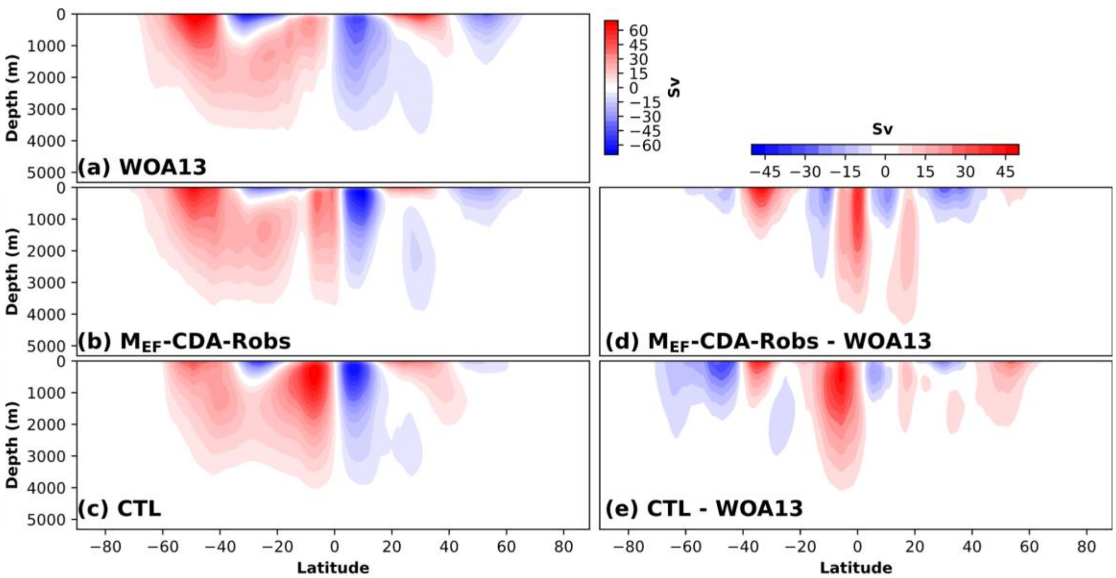

Figure. 16 The climatologically-convergent geostrophic GMOC produced by multiscale ensemble filtering CDA. a-c) The distributions of geostrophic meridional streamfunction derived from WOA13 (panel a), M_{EF}-CDA-Robs-produced (panel b) and free CM2 model control (panel c) climatological temperature and salinity data. d-e) The differences between panels b and a (panel e) as well as between panels c and a (panel f). Note that given coarse vertical discretization in deep ocean, to maintain deep ocean weak geostrophic information, the integral for deriving geostrophic streamfunction is from the bottom to surface.

The goal of this study is to conceptually prove that it is feasible to reconstruct GMOC through combining CGCMs with the Earth observing system, rather than a thorough examination on GMOC reanalysis, requiring exhausted analyses for a long time CDA products which is one of our undergoing projects. Through the analyses above, we may conclude that within a CDA framework, simultaneously working with atmospheric data constraints, a sound multiscale oceanic data constrain that makes oceanic variables having a correct vertical structure is able to produce a reliable GMOC estimation in terms of time mean structure. Once convergent variability in coupled reanalysis with multiple CGCMs using the multiscale CDA algorithm is detected, based on such multi-model multiscale ensemble filtering CDA systems, the probabilistic seamless prediction from seasonal-interannual to multidecadal scales becomes practical.

7 Summary and Discussion

With aids of two CGCMs which are biased with respect to each other, we designed a biased "twin" experiment framework to study the issue of GMOC estimation by incorporating observations into a CGCM. One of two CGCMs is used to create a "true" solution of GMOC estimation and sample the "observations" based on the realistic observing network. As the "observations" are assimilated into the other model to recover the "truth," the degree by which the "true" GMOC is recovered is an assessment of successfulness of an assimilation scheme. With two schemes for data-model incorporation (i.e., ensemble of multiscale filtering and ensemble multiscale filtering), we configure ADA (only conducting atmospheric data constraint), ODA (only conducting oceanic data constraint), and CDA which conducts both atmospheric and oceanic data constraints together within the coupled model framework. Then we examine the role and mechanism of atmospheric and oceanic data constraints as well as the impact of coherence of data-model incorporation in GMOC estimation.

We find that for reconstruction of GMOC by incorporating observational information into a coupled model, the following two aspects are very important. Firstly, a sound DA algorithm that can achieve a balanced and coherent data-model incorporation (e.g., taking multiscale ensemble filtering) makes model variables having balanced physical relations and coherent spatial distributions. For oceanic data constraint, recovering a correct vertical structure is critical for retrieving variability and thus such multiscale filtering must include the correction of climatological mean state and seasonal cycle. Secondly, simultaneous data constraints in atmosphere and ocean components during the coupled model integration, which transfer observational information between the atmosphere and ocean through corrected exchange fluxes at air-sea interface, can significantly enhance the balance and coherence of the data-constrained atmosphere and ocean states. Therefore, the multiscale CDA including recovery of ocean climatology which produces balanced air-sea exchange fluxes and coherent ocean vertical water transport is able to reconstruct the GMOC in a large extent.

An accompanying study is conducting an exhausted analysis on climate variability of a few decades in coupled reanalyses with converged behaviors including GMOC produced by CESM and CM2 CDA systems using the multiscale CDA algorithm. That could serve as a solid sustenance for seamless seasonal-interannual to multidecadal predictability studies. Follow-up studies also include the extension of multi-model coupled reanalysis to century scales for facilitating deeper detection of GMOC variability and mechanism. Based on such multi-model multiscale ensemble filtering CDA systems, establishment of probabilistic seamless predictions from seasonal-interannual to multidecadal scales is also in the priority.

However, given the high sensitivities of GMOC estimation on spatial coherence of ocean states, the high-accuracy coupled reanalysis with better GMOC estimation still has a big space for improvement, for which the multi-model seamless ensemble prediction system can serve as a test platform. In the future, great lights shall be darted on improving coupled modeling and ocean estimation with incorporation of model and more observational information that represents richer scales of ocean motions. By that way, more physical balance among ocean temperature, salinity and currents as well as their spatial coherence, especially for the vertical structure of temperature and salinity, can be gained and maintained. This requires four aspects of efforts for advancing coupled reanalysis.

First, in general, the ocean observing system in the history has far imperfect representation for the real ocean system (*Abraham et al.*, 2013), even for the modern Argo system which still has a big space for improvement (*Roemmich et al.*, 2009). Second, significant modeling errors exist in ocean and coupled system models (*S Zhang et al.*, 2023). One of outstanding issues is insufficient tropical high frequency air-sea interaction (*Bernie et al.*, 2005; *Marullo et al.*, 2016; *H Zhang et al.*, 2018) which can have significant impacts on GMOC simulation (Gnanadesikan, 1999). Third, the behaviors of oceans at polar regions have big impacts on GMOC (*Li et al.*, 2021; *Oka et al.*, 2021), for which sea ice plays an important role. Currently sea ice data assimilation is not included in the CDA system yet, whose impacts on ocean state estimation has been proved in the previous studies (*Liu et al.*, 2021). Therefore, follow-up studies shall consider improvement of sea-ice estimation which incorporates multitype of sea-ice observations with more physical balance and coherence with the atmospheric and oceanic data constraints (*Wu et al.*, 2016; *S. Zhang et al.*, 2013). Finally, refinement of deep ocean bias constraint with high-resolution coupled modeling (*S Zhang et al.*, 2023) and data assimilation (*Li et al.*, 2021) is necessary for creating a creditable coupled reanalysis dataset which has a credible GMOC. Then, the seamless weather-climate prediction of daily to multidecadal scales becomes feasible.

Acknowledgments

The authors would like to thank Prof. Xianyao Chen for his helpful discussion on AMOC background information. This research was supported by National Key R&D Program of China (2022YFE0106400), Science and Technology Innovation Project of Laoshan Laboratory (No. LSKJ202202200, LSKJ202202201, LSKJ202202202, LSKJ202202203, LSKJ202202204), the National Natural Science Foundation of China (41830964, 42022041, 42288101, 41876001), Shandong Province's “Taishan” Scientist Program (ts201712017).

Open Research

The code of CESM1.3 (*Small et al.*, 2014) and CM2.1 (*Delworth et al.*, 2006) is available at https://www.cesm.ucar.edu/ and https://www.gfdl.noaa.gov/cm2-5-and-flor-quickstart/, respectively. The ERA5 reanalysis data are available from the Copernicus Climate Change Service (C3S) Climate Data Store (CDA) (*Hersbach et al.*, 2020), the OISST (*B Huang et al.*, 2021), World Ocean Dataset (WOD) (*Boyer et al.*, 2009) and World Ocean Atlas (WOA) (Locarnini et al., 2013; Zweng et al., 2013) data is obtained from National Oceanic and Atmospheric Administration (NOAA) website (https://www.ncei.noaa.gov/products). The Argo data (*Wong et al.*, 2020) is available at ftp://ftp.ifremer.fr/ifremer/argo/geo. The HadISST (*Rayner et al.*, 2003) can be accessed in https://www.metoffice.gov.uk/hadobs/hadisst. Since the data used to produce the figures and analyses in this work are very large, they can be obtained by sending request to the corresponding author.

References

Abraham, J. P., et al. (2013), A review of global ocean temperature observations: Implications for ocean heat content estimates and climate change, *Reviews of Geophysics*, *51*(3), 450-483, doi:https://doi.org/10.1002/rog.20022.

Anderson, J. L. (2003), A Local Least Squares Framework for Ensemble Filtering, *Monthly Weather Review*, *131*(4), 634-642, doi:https://doi.org/10.1175/1520-0493(2003)131<0634:ALLSFF>2.0.CO;2.

Badin, G., and R. G. Williams (2010), On the Buoyancy Forcing and Residual Circulation in the Southern Ocean: The Feedback from Ekman and Eddy Transfer, *Journal of Physical Oceanography*, *40*(2), 295-310, doi:https://doi.org/10.1175/2009JPO4080.1.

Balmaseda, M., and D. Anderson (2009), Impact of initialization strategies and observations on seasonal forecast skill, *Geophysical Research Letters*, *36*(1), doi:https://doi.org/10.1029/2008GL035561.

Bernie, D. J., E. Guilyardi, G. Madec, J. M. Slingo, and S. J. Woolnough (2007), Impact of resolving the diurnal cycle in an ocean–atmosphere GCM. Part 1: a diurnally forced OGCM, *Climate Dynamics*, *29*(6), 575-590, doi:10.1007/s00382-007-0249-6.

Bernie, D. J., S. J. Woolnough, J. M. Slingo, and E. Guilyardi (2005), Modeling Diurnal and Intraseasonal Variability of the Ocean Mixed Layer, *Journal of Climate*, *18*(8), 1190-1202, doi:https://doi.org/10.1175/JCLI3319.1.

Bingham, R. J., C. W. Hughes, V. Roussenov, and R. Williams (2007), Meridional coherence of the North Atlantic meridional overturning circulation, *Geophysical Research Letters*, *34*(23).

Bjerknes, J. (1964), Atlantic Air-Sea Interaction, in *Advances in Geophysics*, edited by H. E. Landsberg and J. Van Mieghem, pp. 1-82, Elsevier, doi:https://doi.org/10.1016/S0065-2687(08)60005-9.

Boyer, T. P., J. I. Antonov, O. K. Baranova, H. E. Garcia, D. R. Johnson, A. V. Mishonov, T. D. O'Brien, D. Seidov, I. Smolyar, and M. M. Zweng (2009), World ocean database 2009 [Dataset].

Carrassi, A., M. Bocquet, L. Bertino, and G. Evensen (2018), Data assimilation in the geosciences: An overview of methods, issues, and perspectives, *Wiley Interdisciplinary Reviews: Climate Change*, *9*(5), e535.

Cheng, L., H. Luo, T. Boyer, R. Cowley, J. Abraham, V. Gouretski, F. Reseghetti, and J. Zhu (2018), How Well Can We Correct Systematic Errors in Historical XBT Data?, *Journal of Atmospheric and Oceanic Technology*, *35*(5), 1103-1125, doi:https://doi.org/10.1175/JTECH-D-17-0122.1.

Chu, P. C. (2000), P-Vector Spirals and Determination of Absolute Velocities, *Journal of Oceanography*, *56*(5), 591-599, doi:10.1023/A:1011161313505.

Chu, P. C., and C. W. Fan (2015), Absolute geostrophic velocity inverted from World Ocean Atlas 2013 (WOAV13) with the P-vector method, *Geoscience Data Journal*, *2*(2), 78-82, doi:https://doi.org/10.1002/gdj3.31.

Cronin, M. F., et al. (2019), Air-Sea Fluxes With a Focus on Heat and Momentum, *Frontiers in Marine Science*, *6*, doi:10.3389/fmars.2019.00430.

Cunningham, S. A., T. Kanzow, D. Rayner, M. O. Baringer, W. E. Johns, J. Marotzke, H. R. Longworth, E. M. Grant, J. J.-M. Hirschi, and L. Beal (2007), Temporal variability of the Atlantic meridional overturning circulation at 26.5 N, *Science*, *317*(5840), 935-938.

Danabasoglu, G., J. C. McWilliams, and P. R. Gent (1994), The Role of Mesoscale Tracer Transports in the Global Ocean Circulation, *Science*, *264*(5162), 1123-1126, doi:10.1126/science.264.5162.1123.

Danabasoglu, G., S. G. Yeager, D. Bailey, E. Behrens, M. Bentsen, D. Bi, A. Biastoch, C. Böning, A. Bozec, and V. M. Canuto (2014), North Atlantic simulations in coordinated ocean-ice reference experiments phase II (CORE-II). Part I: mean states, *Ocean Modelling*, *73*, 76-107.

Danabasoglu, G., S. G. Yeager, W. M. Kim, E. Behrens, M. Bentsen, D. Bi, A. Biastoch, R. Bleck, C. Böning, and A. Bozec (2016), North Atlantic simulations in Coordinated Ocean-ice Reference Experiments phase II (CORE-II). Part II: Inter-annual to decadal variability, *Ocean Modelling*, *97*, 65-90.

Dee, D. P. (2005), Bias and data assimilation, *Quarterly Journal of the Royal Meteorological Society*, *131*(613), 3323-3343, doi:https://doi.org/10.1256/qj.05.137.

Dee, D. P., and A. M. Da Silva (1998), Data assimilation in the presence of forecast bias, *Quarterly Journal of the Royal Meteorological Society*, *124*(545), 269-295, doi:https://doi.org/10.1002/qj.49712454512.

Delworth, T. L., et al. (2006), GFDL's CM2 Global Coupled Climate Models. Part I: Formulation and Simulation Characteristics [Software], *Journal of Climate*, *19*(5), 643-674, doi:https://doi.org/10.1175/JCLI3629.1.

Delworth, T. L., and F. Zeng (2016), The Impact of the North Atlantic Oscillation on Climate through Its Influence on the Atlantic Meridional Overturning Circulation, *Journal of Climate*, *29*(3), 941-962, doi:https://doi.org/10.1175/JCLI-D-15-0396.1.

Evensen, G., F. C. Vossepoel, and P. J. van Leeuwen (2022), Fully Nonlinear Data Assimilation, in *Data Assimilation Fundamentals: A Unified Formulation of the State and Parameter Estimation Problem*, edited, pp. 95-110, Springer.

Eyring, V., S. Bony, G. A. Meehl, C. A. Senior, B. Stevens, R. J. Stouffer, and K. E. Taylor (2016), Overview of the Coupled Model Intercomparison Project Phase 6 (CMIP6) experimental design and organization, *Geosci. Model Dev.*, *9*(5), 1937-1958, doi:10.5194/gmd-9-1937-2016.

Fairall, C. W., E. F. Bradley, D. P. Rogers, J. B. Edson, and G. S. Young (1996), Bulk parameterization of air-sea fluxes for Tropical Ocean-Global Atmosphere Coupled-Ocean Atmosphere Response Experiment, *Journal of Geophysical Research: Oceans*, *101*(C2), 3747-3764, doi:https://doi.org/10.1029/95JC03205.

Ganachaud, A., and C. Wunsch (2000), Improved estimates of global ocean circulation, heat transport and mixing from hydrographic data, *Nature*, *408*(6811), 453-457.

Gnanadesikan, A. (1999), A Simple Predictive Model for the Structure of the Oceanic Pycnocline, *Science*, *283*(5410), 2077-2079, doi:10.1126/science.283.5410.2077.

Gnanadesikan, A., et al. (2006), GFDL's CM2 Global Coupled Climate Models. Part II: The Baseline Ocean Simulation, *Journal of Climate*, *19*(5), 675-697, doi:https://doi.org/10.1175/JCLI3630.1.

Hersbach, H., et al. (2020), The ERA5 global reanalysis [Dataset], *Quarterly Journal of the Royal Meteorological Society*, *146*(730), 1999-2049, doi:https://doi.org/10.1002/qj.3803.

Hirschi, J. J.-M., et al. (2020), The Atlantic Meridional Overturning Circulation in High-Resolution Models, *125*(4), e2019JC015522, doi:https://doi.org/10.1029/2019JC015522.

Hopkins, T. S. (1991), The GIN Sea—A synthesis of its physical oceanography and literature review 1972–1985, *Earth-Science Reviews*, *30*(3), 175-318, doi:https://doi.org/10.1016/0012-8252(91)90001-V.

Huang, B., C. Liu, V. Banzon, E. Freeman, G. Graham, B. Hankins, T. Smith, and H.-M. Zhang (2021), Improvements of the Daily Optimum Interpolation Sea Surface Temperature (DOISST) Version 2.1, *Journal of Climate*, *34*(8), 2923-2939, doi:https://doi.org/10.1175/JCLI-D-20-0166.1.

Huang, R. X., W. Wang, and L. L. Liu (2006), Decadal variability of wind-energy input to the world ocean, *Deep Sea Research Part II: Topical Studies in Oceanography*, *53*(1), 31-41, doi:https://doi.org/10.1016/j.dsr2.2005.11.001.

Hunke, E. C., W. H. Lipscomb, A. K. Turner, N. Jeffery, and S. Elliott (2010), Cice: the los alamos sea ice model documentation and software user's manual version 4.1 la-cc-06-012, *T-3 Fluid Dynamics Group, Los Alamos National Laboratory*, *675*, 500, doi:https://svn-ccsm-models.cgd.ucar.edu/cesm1/alphas/branches/cesm1_5_alpha04c_timers/components/cice/src/doc/cicedoc.pdf.

Jazwinski, A. H. (2007), *Stochastic processes and filtering theory*, Courier Corporation.

Johnson, G. C., et al. (2021), Global Oceans, *Bulletin of the American Meteorological Society*, *102*(8), S143-S198, doi:https://doi.org/10.1175/BAMS-D-21-0083.1.

Johnson, H. L., P. Cessi, D. P. Marshall, F. Schloesser, and M. A. J. J. o. G. R. O. Spall (2019), Recent contributions of theory to our understanding of the Atlantic meridional overturning circulation, *124*(8), 5376-5399.

Karspeck, A. R., et al. (2017), Comparison of the Atlantic meridional overturning circulation between 1960 and 2007 in six ocean reanalysis products, *Climate Dynamics*, *49*(3), 957-982, doi:10.1007/s00382-015-2787-7.

Karsten, R. H., and J. Marshall (2002), Constructing the Residual Circulation of the ACC from Observations, *Journal of Physical Oceanography*, *32*(12), 3315-3327, doi:https://doi.org/10.1175/1520-0485(2002)032<3315:CTRCOT>2.0.CO;2.

Lee, S.-K., R. Lumpkin, M. O. Baringer, C. S. Meinen, M. Goes, S. Dong, H. Lopez, and S. G. Yeager (2019), Global Meridional Overturning Circulation Inferred From a Data-Constrained Ocean & Sea-Ice Model, *Geophysical Research Letters*, *46*(3), 1521-1530, doi:https://doi.org/10.1029/2018GL080940.

Lee, S.-K., R. Lumpkin, F. Gomez, S. Yeager, H. Lopez, F. Takglis, S. Dong, W. Aguiar, D. Kim, and M. Baringer (2023), Human-induced changes in the global meridional overturning circulation are emerging from the Southern Ocean, *Communications Earth & Environment*, *4*(1), 69, doi:10.1038/s43247-023-00727-3.

Li, H., A. Fedorov, and W. Liu (2021), AMOC Stability and Diverging Response to Arctic Sea Ice Decline in Two Climate Models, *Journal of Climate*, *34*(13), 5443-5460, doi:https://doi.org/10.1175/JCLI-D-20-0572.1.

Lin, S.-J. (2004), A "Vertically Lagrangian" Finite-Volume Dynamical Core for Global Models, *Monthly Weather Review*, *132*(10), 2293-2307, doi:https://doi.org/10.1175/1520-0493(2004)132<2293:AVLFDC>2.0.CO;2.

Liu, X., et al. (2021), Development of Coupled Data Assimilation With the BCC Climate System Model: Highlighting the Role of Sea-Ice Assimilation for Global Analysis, *Journal of Advances in Modeling Earth Systems*, *13*(4), e2020MS002368, doi:https://doi.org/10.1029/2020MS002368.

Locarnini, R. A., A. V. Mishonov, J. I. Antonov, T. P. Boyer, H. E. Garcia, O. K. Baranova, M. M. Zweng, C. R. Paver, J. R. Reagan, D. R. Johnson, M. Hamilton, and D. Seidov, 2013. World Ocean Atlas 2013 [Dataset], Volume 1: Temperature. S. Levitus, Ed., A. Mishonov Technical Ed.; NOAA Atlas NESDIS 73, 40 pp.

Lozier, M. S., S. Bacon, A. S. Bower, S. A. Cunningham, M. F. de Jong, L. de Steur, B. Deyoung, J. Fischer, S. F. Gary, and B. J. Greenan (2017), Overturning in the Subpolar North Atlantic Program: A new international ocean observing system, *Bulletin of the American Meteorological Society*, *98*(4), 737-752.

Lu, L., et al. (2023), An Improved Coupled Data Assimilation System with a CGCM Using Multi-Time-Scale High-Efficiency EnOI-Like Filtering *Journal of Climate*, *36*(17), 6045-6067, doi:https://doi.org/10.1175/JCLI-D-22-0558.1.

Lu, L., S. Zhang, S. G. Yeager, G. Danabasoglu, P. Chang, L. Wu, X. Lin, A. Rosati, and F. Lu (2020), Impact of coherent ocean stratification on AMOC reconstruction by coupled data assimilation with a biased model, *Journal of Climate*, *33*(17), 7319-7334.

Lumpkin, R., and K. Speer (2003), Large-scale vertical and horizontal circulation in the North Atlantic Ocean, *Journal of Physical Oceanography*, *33*(9), 1902-1920.

Ma, X., et al. (2016), Western boundary currents regulated by interaction between ocean eddies and the atmosphere, *Nature*, *535*(7613), 533-537, doi:10.1038/nature18640.

Macdonald, A. M., and C. Wunsch (1996), An estimate of global ocean circulation and heat fluxes, *Nature*, *382*(6590), 436-439, doi:10.1038/382436a0.

Manabe, S. (1969), CLIMATE AND THE OCEAN CIRCULATION: I. THE ATMOSPHERIC CIRCULATION AND THE HYDROLOGY OF THE EARTH'S SURFACE, *Monthly Weather Review*, *97*(11), 739-774, doi:https://doi.org/10.1175/1520-0493(1969)097<0739:CATOC>2.3.CO;2.

Marullo, S., P. J. Minnett, R. Santoleri, and M. Tonani (2016), The diurnal cycle of sea-surface temperature and estimation of the heat budget of the Mediterranean Sea, *Journal of Geophysical Research: Oceans*, *121*(11), 8351-8367, doi:https://doi.org/10.1002/2016JC012192.

McIntosh, P. C., and T. J. McDougall (1996), Isopycnal Averaging and the Residual Mean Circulation, *Journal of Physical Oceanography*, *26*(8), 1655-1660, doi:https://doi.org/10.1175/1520-0485(1996)026<1655:IAATRM>2.0.CO;2.

McPhaden, M. J., et al. (1998), The Tropical Ocean-Global Atmosphere observing system: A decade of progress, *Journal of Geophysical Research: Oceans*, *103*(C7), 14169-14240, doi:https://doi.org/10.1029/97JC02906.

Meehl, G. A., et al. (2019), Effects of Model Resolution, Physics, and Coupling on Southern Hemisphere Storm Tracks in CESM1.3, *Geophysical Research Letters*, *46*(21), 12408-12416, doi:https://doi.org/10.1029/2019GL084057.

Mercier, H., et al. (2015), Variability of the meridional overturning circulation at the Greenland–Portugal OVIDE section from 1993 to 2010, *Progress in Oceanography*, *132*, 250-261, doi:https://doi.org/10.1016/j.pocean.2013.11.001.

Munk, W. (1950), ON THE WIND-DRIVEN OCEAN CIRCULATION, *Journal of Atmospheric Sciences*, *7*(2), 80-93, doi:https://doi.org/10.1175/1520-0469(1950)007<0080:OTWDOC>2.0.CO;2.

Munk, W., and C. Wunsch (1998), Abyssal recipes II: energetics of tidal and wind mixing, *Deep Sea Research Part I: Oceanographic Research Papers*, *45*(12), 1977-2010, doi:https://doi.org/10.1016/S0967-0637(98)00070-3.

Nikurashin, M., and G. Vallis (2012), A theory of the interhemispheric meridional overturning circulation and associated stratification, *Journal of Physical Oceanography*, *42*(10), 1652-1667.

Oka, A., A. Abe-Ouchi, S. Sherriff-Tadano, Y. Yokoyama, K. Kawamura, and H. Hasumi (2021), Glacial mode shift of the Atlantic meridional overturning circulation by warming over the Southern Ocean, *Communications Earth & Environment*, *2*(1), 169, doi:10.1038/s43247-021-00226-3.

Osborn, T. R. (1980), Estimates of the Local Rate of Vertical Diffusion from Dissipation Measurements, *Journal of Physical Oceanography*, *10*(1), 83-89, doi:https://doi.org/10.1175/1520-0485(1980)010<0083:EOTLRO>2.0.CO;2.

Penny, S. G., and T. M. Hamill (2017), COUPLED DATA ASSIMILATION FOR INTEGRATED EARTH SYSTEM ANALYSIS AND PREDICTION, *Bulletin of the American Meteorological Society*, *98*(7), ES169-ES172.

Perez, F. F., et al. (2018), Meridional overturning circulation conveys fast acidification to the deep Atlantic Ocean, *Nature*, *554*(7693), 515-518, doi:10.1038/nature25493.

Philander, S. G. (1990), *El Niño, La Niña, and the Southern Oscillation (International Geophysics Series; V. 46)*, Academic Press.

Pickart, R. S., and M. A. Spall (2007), Impact of Labrador Sea Convection on the North Atlantic Meridional Overturning Circulation, *Journal of Physical Oceanography*, *37*(9), 2207-2227, doi:https://doi.org/10.1175/JPO3178.1.

Price, J. F., R. A. Weller, and R. R. Schudlich (1987), Wind-Driven Ocean Currents and Ekman Transport, *Science*, *238*(4833), 1534-1538, doi:10.1126/science.238.4833.1534.

Rayner, N. A., D. E. Parker, E. B. Horton, C. K. Folland, L. V. Alexander, D. P. Rowell, E. C. Kent, and A. Kaplan (2003), Global analyses of sea surface temperature, sea ice, and night marine air temperature since the late nineteenth century [Dataset], *Journal of Geophysical Research: Atmospheres*, *108*(D14), doi:https://doi.org/10.1029/2002JD002670.

Rintoul, S. R. (2018), The global influence of localized dynamics in the Southern Ocean, *Nature*, *558*(7709), 209-218, doi:10.1038/s41586-018-0182-3.

Roemmich, D., G. C. Johnson, S. Riser, R. Davis, J. Gilson, W. B. Owens, S. L. Garzoli, C. Schmid, and M. Ignaszewski (2009), The Argo Program
Observing the Global Ocean with Profiling Floats, *Oceanography*, *22*(2), 34-43.

Sévellec, F., and S. S. Drijfhout (2018), A novel probabilistic forecast system predicting anomalously warm 2018-2022 reinforcing the long-term global warming trend, *Nature Communications*, *9*(1), 3024, doi:10.1038/s41467-018-05442-8.

Shaffrey, L., and R. Sutton (2006), Bjerknes Compensation and the Decadal Variability of the Energy Transports in a Coupled Climate Model, *Journal of Climate*, *19*(7), 1167-1181, doi:https://doi.org/10.1175/JCLI3652.1.

Small, R. J., et al. (2014), A new synoptic scale resolving global climate simulation using the Community Earth System Model [Software], *Journal of Advances in Modeling Earth Systems*, *6*(4), 1065-1094, doi:https://doi.org/10.1002/2014MS000363.

Stommel, H. (1961), Thermohaline Convection with Two Stable Regimes of Flow, *Tellus*, *13*(2), 224-230, doi:https://doi.org/10.1111/j.2153-3490.1961.tb00079.x.

Sugiura, N., T. Awaji, S. Masuda, T. Mochizuki, T. Toyoda, T. Miyama, H. Igarashi, and Y. Ishikawa (2008), Development of a four-dimensional variational coupled data assimilation system for enhanced analysis and prediction of seasonal to interannual climate variations, *Journal of Geophysical Research: Oceans*, *113*(C10), doi:https://doi.org/10.1029/2008JC004741.

Sun, J., Y. Jiang, S. Zhang, W. Zhang, L. Lu, G. Liu, Y. Chen, X. Xing, X. Lin, and L. Wu (2022), An online ensemble coupled data assimilation capability for the Community Earth System Model: system design and evaluation, *Geosci. Model Dev.*, *15*(12), 4805-4830, doi:10.5194/gmd-15-4805-2022.

Sverdrup, H. U., M. W. Johnson, and R. H. Fleming (1942), *The Oceans: Their physics, chemistry, and general biology*, Prentice-Hall New York.

Taylor, K. E., R. J. Stouffer, and G. A. Meehl (2012), An Overview of CMIP5 and the Experiment Design, *Bulletin of the American Meteorological Society*, *93*(4), 485-498, doi:https://doi.org/10.1175/BAMS-D-11-00094.1.

Thompson, J. D. (1978), Role of Mixing in the Dynamics of Upwelling Systems, paper presented at Upwelling Ecosystems, Springer Berlin Heidelberg, Berlin, Heidelberg, 1978//.

Visbeck, M., J. Marshall, T. Haine, and M. Spall (1997), Specification of Eddy Transfer Coefficients in Coarse-Resolution Ocean Circulation Models, *Journal of Physical Oceanography*, *27*(3), 381-402, doi:https://doi.org/10.1175/1520-0485(1997)027<0381:SOETCI>2.0.CO;2.

Winton, M. (2000), A Reformulated Three-Layer Sea Ice Model, *Journal of Atmospheric and Oceanic Technology*, *17*(4), 525-531, doi:https://doi.org/10.1175/1520-0426(2000)017<0525:ARTLSI>2.0.CO;2.

Wong, A. P., et al. (2020), Argo data 1999–2019: Two million temperature-salinity profiles and subsurface velocity observations from a global array of profiling floats[Dataset], *Frontiers in Marine Science*, *7*, 700.

Wright, D. G., and T. F. Stocker (1991), A Zonally Averaged Ocean Model for the Thermohaline Circulation. Part I: Model Development and Flow Dynamics, *Journal of Physical Oceanography*, *21*(12), 1713-1724, doi:https://doi.org/10.1175/1520-0485(1991)021<1713:AZAOMF>2.0.CO;2.

Wright, D. G., T. F. Stocker, and D. Mercer (1998), Closures Used in Zonally Averaged Ocean Models, *Journal of Physical Oceanography*, *28*(5), 791-804, doi:https://doi.org/10.1175/1520-0485(1998)028<0791:CUIZAO>2.0.CO;2.

Wu, X., S. Zhang, and Z. Liu (2016), Implementation of a one-dimensional enthalpy sea-ice model in a simple pycnocline prediction model for sea-ice data assimilation studies, *Advances in Atmospheric Sciences*, *33*(2), 193-207, doi:10.1007/s00376-015-5099-2.

Wunsch, C., and R. Ferrari (2004), Vertical mixing, energy, and the general circulation of the oceans, *Annu. Rev. Fluid Mech.*, *36*, 281-314.

Yang, D., Y. Tang, X.-Q. Yang, X. Song, X. Tan, Y. Wu, X. Yan, T. Liu, and X. Sun (2023), Probabilistic versus deterministic potential seasonal climate predictability under the perfect-model framework, *Climate Dynamics*, *61*(9), 4429-4447, doi:10.1007/s00382-023-06814-7.

Yang, H., Y. Wang, and Z. Liu (2013), A modelling study of the Bjerknes compensation in the meridional heat transport in a freshening ocean, *Tellus A: Dynamic Meteorology and Oceanography*, *65*(1), 18480, doi:10.3402/tellusa.v65i0.18480.

Yang, T., and Y. Xu (2015), Estimation of the time series of the meridional heat transport across 15° N in the P acific O cean from A rgo and satellite data, *ournal of Geophysical Research: Oceans*, *120*(4), 3043-3060.

Yu, X., S. Zhang, J. Li, L. Lu, Z. Liu, M. Li, H. Yu, G. Han, X. Lin, and L. Wu (2019), A Multi‐Timescale EnOI‐Like High‐Efficiency Approximate Filter for Coupled Model Data Assimilation, *Journal of Advances in Modeling Earth Systems*, *11*(1), 45-63.

Zhang, H., H. Beggs, C. J. Merchant, X. H. Wang, L. Majewski, A. E. Kiss, J. Rodríguez, L. Thorpe, C. Gentemann, and M. Brunke (2018), Comparison of SST Diurnal Variation Models Over the Tropical Warm Pool Region, *Journal of Geophysical Research: Oceans*, *123*(5), 3467-3488, doi:https://doi.org/10.1029/2017JC013517.

Zhang, R., R. Sutton, G. Danabasoglu, Y. O. Kwon, R. Marsh, S. G. Yeager, D. E. Amrhein, and C. M. J. R. o. G. Little (2019), A review of the role of the Atlantic meridional overturning circulation in Atlantic multidecadal variability and associated climate impacts, *57*(2), 316-375.

Zhang, S. (2011), Impact of observation-optimized model parameters on decadal predictions: Simulation with a simple pycnocline prediction model, *Geophysical Research Letters*, *38*(2), doi:https://doi.org/10.1029/2010GL046133.

Zhang, S., Y. S. Chang, X. Yang, and A. Rosati (2014), Balanced and Coherent Climate Estimation by Combining Data with a Biased Coupled Model, *Journal of Climate*, *27*(3), 1302-1314, doi:https://doi.org/10.1175/JCLI-D-13-00260.1.

Zhang, S., M. J. Harrison, A. Rosati, and A. Wittenberg (2007), System Design and Evaluation of Coupled Ensemble Data Assimilation for Global Oceanic Climate Studies, *Monthly Weather Review*, *135*(10), 3541-3564, doi:https://doi.org/10.1175/MWR3466.1.

Zhang, S., Z. Liu, X. Zhang, X. Wu, G. Han, Y. Zhao, X. Yu, C. Liu, Y. Liu, and S. Wu (2020), Coupled data assimilation and parameter estimation in coupled ocean–atmosphere models: a review, *Climate Dynamics*, *54*, 5127-5144.

Zhang, S., A. Rosati, and M. J. Harrison (2009), Detection of multidecadal oceanic variability by ocean data assimilation in the context of a “perfect” coupled model, *Journal of Geophysical Research: Oceans*, *114*(C12), doi:https://doi.org/10.1029/2008JC005261.

Zhang, S., M. Winton, A. Rosati, T. Delworth, and B. Huang (2013), Impact of Enthalpy-Based Ensemble Filtering Sea Ice Data Assimilation on Decadal Predictions: Simulation with a Conceptual Pycnocline Prediction Model *Journal of Climate*, *26*(7), 2368-2378, doi:https://doi.org/10.1175/JCLI-D-11-00714.1.

Zhang, S., et al. (2023), Toward Earth system modeling with resolved clouds and ocean submesoscales on heterogeneous many-core HPCs, *National Science Review*, *10*(6), nwad069, doi:10.1093/nsr/nwad069.

Zweng, M.M, J.R. Reagan, J.I. Antonov, R.A. Locarnini, A.V. Mishonov, T.P. Boyer, H.E. Garcia, O.K. Baranova, D.R. Johnson, D.Seidov, M.M. Biddle, 2013. World Ocean Atlas 2013 [Dataset], Volume 2: Salinity. S. Levitus, Ed., A. Mishonov Technical Ed.; NOAA Atlas NESDIS 74, 39 pp.